High-resolution numerical assessment of large-scale riverine alkalinity modification scenarios along the southern coast of the United States

Xing Zhou[1, *], Annalisa Bracco[1, 2], Takamitsu Ito[1], Christopher T. Reinhard[1]
[1]School of Earth and Atmospheric Sciences, Georgia Institute of Technology, USA
[2]CMCC Foundation, Euro-Mediterranean Center on Climate Change, Italy.

*Corresponding Author: xzhou473@gatech.edu

Abstract: River-based alkalinity modifications represent potentially effective approaches for removing atmospheric CO_2 and mitigating anthropogenic climate change. Evaluating their effectiveness requires consideration of downstream impacts on coastal ocean CO_2 air–sea exchange following intervention. In this study, we applied a high-resolution (5 km) regional coupled physical and biogeochemical model (CROCO-PISCES) to assess two carbon dioxide removal approaches, alkalinity enhancement (AE) and enhanced weathering (EW), in the northern portion of the Gulf of Mexico. Alkalinity and dissolved inorganic carbon inputs were added to riverine outflow from the Mississippi and Atchafalaya Rivers according to eight hypothetical scenarios with variable magnitude and timing. In the AE scenarios, simulations showed oceanic CO_2 uptake efficiencies ranging from 58% to 85%, with higher values under modest perturbations and summer additions when shallow mixed layers promoted near-surface retention of added alkalinity. In the EW scenarios, simulations indicated that 12–15% of land-based carbon sequestration was re-emitted to the atmosphere from the ocean, with the amount remaining largely consistent across scenarios, suggesting that the ocean-side leakage is relatively stable in the EW case and represents a relatively small component of the overall EW life cycle. Collectively, these findings demonstrate that the long-term carbon removal efficiency of river-based alkalinity modification will often depend on the ratio between alkalinity and dissolved organic carbon introduced to the coastal ocean.

Plain Language Summary: Rivers carry large amounts of freshwater and dissolved materials to the ocean, linking land-based carbon processes with the marine environment. These connections make river systems important pathways for carbon dioxide removal strategies. Although these modifications may begin on land or in rivers, their overall climate benefits depend on what happens once the modified water reaches the ocean. In this study, we simulated how increasing alkalinity (representing alkalinity enhancement, AE) or both alkalinity and dissolved inorganic carbon (representing enhanced weathering, EW) in the Mississippi and Atchafalaya Rivers might affect ocean–atmosphere CO_2 exchange in the northern Gulf of Mexico. The simulations investigated scenarios with different magnitudes and timing of river modification. Our results show that AE can strengthen ocean CO_2 uptake, with an efficiency of 58–85% depending on how much and when the alkalinity is added. EW simulations show that about 12–15% of the carbon stored on land is later released back to the atmosphere from the ocean, regardless of the simulated strategies, suggesting that the ocean-side carbon leakage remains relatively stable.

1.Introduction

To stabilize global warming below 2°C above the preindustrial mean temperature, the Intergovernmental Panel on Climate Change (IPCC) has emphasized the necessity of deploying negative emissions technologies alongside deep reductions in greenhouse gas emissions (UNFCCC, 2015; IPCC, 2022). Estimates suggest that achieving this target will require removing approximately 5–10 Gt CO_2 per year

from the atmosphere (IPCC, 2022). These urgent requirements have motivated growing interest in large-scale geoengineering strategies aimed at removing and securely storing atmospheric CO_2 (NASEM, 2019). Examples include ecological-based approaches such as reforestation (Griscom et al., 2017) and blue carbon ecosystem restoration (Duarte et al., 2013; Song et al., 2023), as well as human interventions including enhanced rock weathering (Beerling et al., 2020; Beerling et al., 2025a), ocean alkalinity enhancement and fertilization (Renforth & Henderson, 2017; Babakhani et al., 2022; Zhou et al., 2025).

Oceans and rivers play an important role in the portfolio of carbon dioxide removal approaches. The ocean is the largest long-term carbon reservoir in Earth's surface and the ultimate endpoint of the global water cycle (Ward et al., 2017; Davila et al., 2022; Regnier et al., 2022), and rivers act as natural conveyors linking land-based interventions to coastal seas. As a result, land- and river-based interventions can generate downstream impacts on coastal and open-ocean CO_2 air–sea exchange, and neglecting these effects may bias assessments of their effectiveness. Of particular relevance are approaches such as river-based alkalinity enhancement and enhanced weathering, which alter river alkalinity or dissolved inorganic carbon (DIC) and subsequently influence ocean biogeochemistry and air–sea CO_2 exchange once freshwater plumes enter marine systems.

Alkalinity enhancement (AE) refers to approaches designed to increase the capacity of surface waters to absorb atmospheric CO_2. Examples include reducing seawater acidity through electrochemical processes or adding aqueous alkaline substances such as NaOH or $Ca(OH)_2$ directly to the ocean (Kheshgi 1995; Renforth & Krüger, 2013; Renforth $ Henderson 2017; National Academies of Sciences, Engineering, and Medicine [NASEM], 2021; Eisaman et al., 2023; He & Tyka, 2023). A similar strategy can be applied in rivers by elevating river alkalinity, so that when freshwater plumes enter the ocean, they generate effects comparable to direct ocean additions (Fig. 1a). This river-based approach may be particularly effective in river-dominated coastal regions such as the southern coast of the United States and the northeastern coast of Brazil, where large rivers (e.g., the Mississippi and Amazon) create surface plumes that extend thousands of kilometers offshore (Coles et al., 2013; Mu et al., 2023; Ou et al., 2025). Moreover, river-based AE provides a practical pathway to integrate with wastewater alkalinity enhancement (Li et al., 2025; Zheng et al., 2025), since wastewater treatment plants are built at fixed locations and offer limited deployment flexibility.

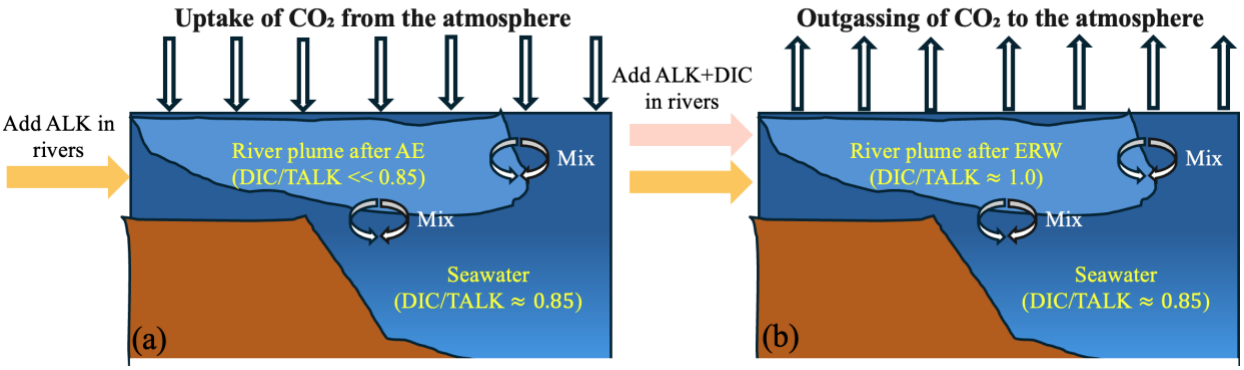

Fig. 1. Conceptual diagram showing changes in the ocean carbonate system following river-based AE(a) and EW (b).

Considerations of AE applications primarily focus on the efficiency of oceanic CO_2 uptake, commonly denoted as η, which is typically defined as the ratio of moles of CO_2 removed from the atmosphere per mole of alkalinity added. This efficiency is influenced by seasonal and spatial variability in ocean dynamics, as well as by the magnitude of the perturbation, since the adjustment timescale of oceanic pCO_2 can range from weeks to years depending on the scale of alkalinity addition (Jones et al., 2014; He & Tyka, 2023; Suseji et al., 2025). At the same time, ocean mixing and transport redistribute both the added alkalinity and the newly formed DIC horizontally and vertically, further modifying efficiency (Fennel et al., 2023; Liu et al., 2025). Together, these processes underscore the fact that designing a feasible AE strategy requires careful consideration of both when it is applied and how it is implemented. In addition, it cannot be assumed that a given amount of alkalinity added will fully equilibrate via atmospheric CO_2 uptake (Zhou et al., 2025), with obvious implications for the monitoring, reporting, and verification (MRV) protocols used to track the impacts of alkalinity modification on carbon markets.

In contrast to AE which is typically designed to directly increase the capacity of the surface ocean to absorb CO_2, enhanced weathering (EW) initially increases the absorption of CO_2 on land (or in rivers), which then causes runoff of added carbon and alkalinity. In this case, potential re-emission of CO_2 from riverine and oceanic systems must be considered (Fig. 1b). EW typically involves pulverizing weatherable rocks (e.g., basalt, olivine, or limestone) and applying them to soils or rivers, where they dissolve and capture atmospheric CO_2 in the form of bicarbonate (Beerling et al., 2020; Kanzaki et al., 2025; Raymond et al., 2025). This bicarbonate can then be transported by rivers and streams to the ocean, where it may remain stored for timescales on the order of 10^4 years (Broecker & Peng, 1987; Archer et al., 1997; Goodwin & Ridgwell, 2010). However, part of the initially captured carbon can be released back to the atmosphere as it interacts with riverine and marine carbonate systems during transit (Cao et al., 2010; Harrington et al., 2023). Using a dynamic river network model, Zhang et al. (2025) estimated a 5–15% carbon loss during riverine transport depending on the location and stream/river transit path. On the ocean side, both the fraction of carbon outgassing and the timescales of this process remain poorly understood. Using an intermediate complexity Earth system model, Kanzaki et al. (2023) estimated a global loss of ~10% for silicate feedstocks and ~20% for carbonate feedstocks when normalized to an equivalent amount of direct air capture. However, no regional ocean modeling studies have yet assessed this leakage or how it may vary under different EW strategies applied at different times and magnitudes.

In this study, we employed a coupled regional ocean and biogeochemistry model (CROCO-PISCES) at 5 km horizontal resolution to evaluate river-based alkalinity modification approaches (AE and EW) in the northern portion of the Gulf of Mexico (hereafter the Northern Gulf). The Northern Gulf provides an ideal testbed for assessing the potential impacts of large-scale, river-based alkalinity modifications, as it is the endpoint of the United States' largest river system (the Mississippi–Atchafalaya River system) and is strongly influenced by anthropogenic activities. In addition, the ocean currents in the Gulf help transport river-derived materials, extending their influence over larger regions. Seasonally varying wind-driven currents favor longshore transport, while the Loop Current - the most intense mesoscale current in the Gulf flowing clockwise into the basin from the Caribbean through the Yucatán Channel, and out of it through the Florida Straits - and its detached eddies facilitate offshore transport (Fig. 2).

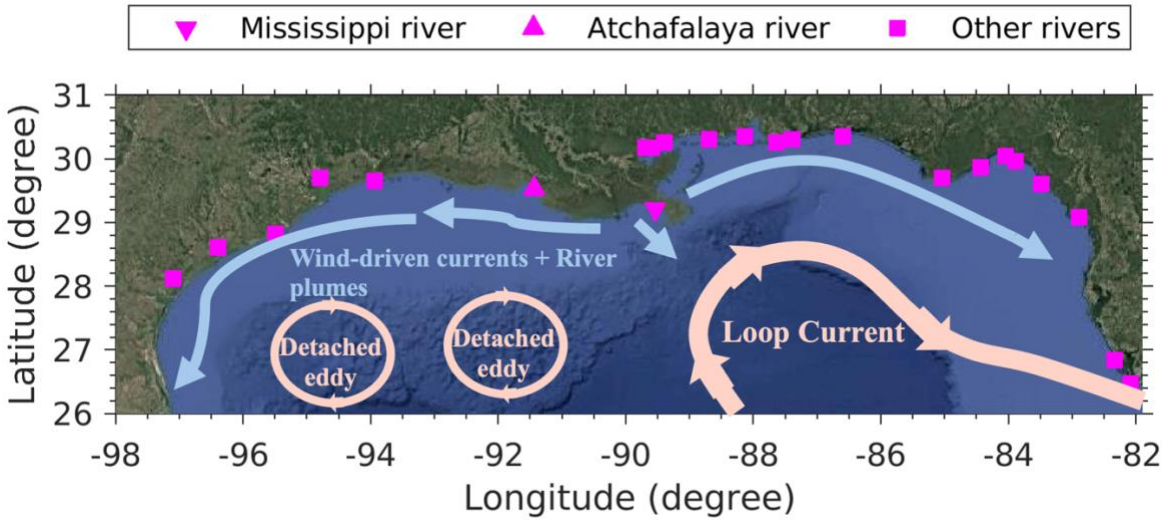

Fig. 2. General circulation features in the Northern Gulf model domain with the river mouths included in the simulations indicated in magenta.

We designed eight scenarios in total to represent idealized AE and EW approaches. These scenarios were structured around addition strategies that varied in the duration of additions (annual versus one month), the magnitude of concentration increases in rivers (10% versus 100%), and the timing of initiation (winter versus summer). For both approaches, we investigated the optimal strategy and the factors influencing it by analyzing simulated air–sea CO_2 exchange dynamics and ocean dynamics in redistributing added materials. This study aims to advance scientific understanding of the efficiency of ocean carbon storage through river-based alkalinity modifications and to inform the development of adaptive and feasible carbon dioxide removal strategies for the southern United States.

2.Method

2.1 Model description

In this study, we applied a regional coupled physical-biogeochemical modeling framework known as CROCO-PISCES. The Coastal and Regional Ocean Community model (CROCO v1.3) is a split-explicit, terrain-following ocean model built upon ROMS-AGRIF (Auclair et al., 2018). It is configured as a free-evolving system designed to study regional, coastal, and nearshore ocean dynamics. Previous studies have demonstrated the ability of CROCO to realistically capture mesoscale variability and circulation features in the Northern Gulf (Liu et al., 2021a; Liu et al., 2022; Sun et al., 2022). The realistic representation of physical transport has supported its application in studies of coral reef and fish larval connectivity (Zhou et al., 2024; Lopera et al., 2025), underscoring the model's utility for ecosystem-scale research.

The biogeochemical module, PISCES, has been coupled to several ocean and Earth system modeling platforms (NEMO, CROCO, IPSL-CM, CNRM-CM, and EC-Earth). In its standard implementation it includes four nutrients (phosphorus, nitrogen, silica, and iron), two phytoplankton groups (nanophytoplankton and diatoms), two zooplankton groups (microzooplankton and mesozooplankton), and a detritus pool consisting of dissolved organic matter, small particles, and large particles (Fig. 3a). This structure enables PISCES to effectively describe the biogeochemical cycles of nutrients, carbon, and oxygen. A comprehensive description of the PISCES model can be found in Aumont et al. (2015).

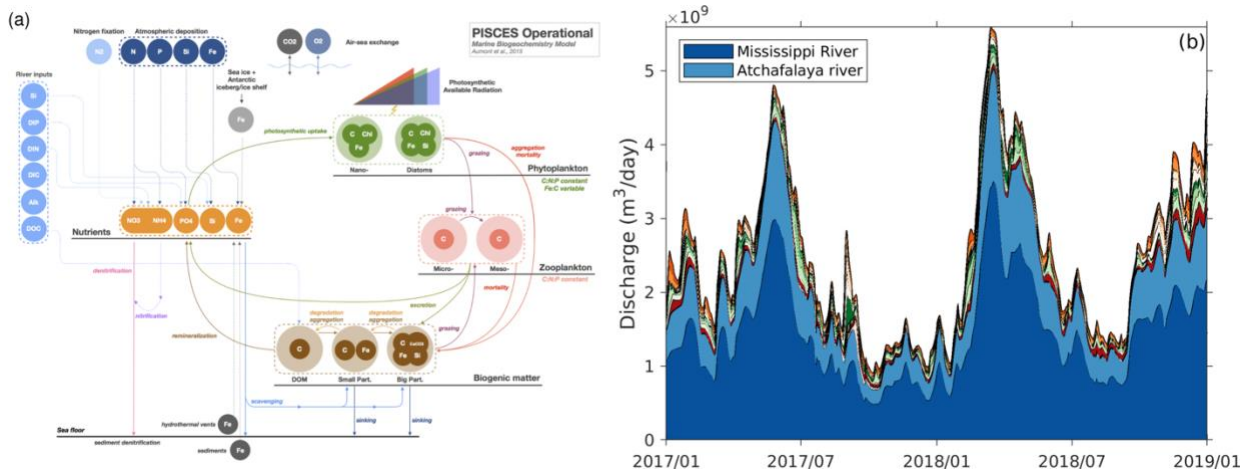

Fig. 3. (a) Schematic diagram of the standard "Operational" version of PISCES (adapted from https://www.pisces-community.org/index.php/model-description/). (b) Daily freshwater discharge rates of all rivers flowing into the Gulf during 2017 and 2018, highlighting the dominant contributions of the Mississippi and Atchafalaya Rivers.

2.2 Model configuration

The CROCO-PISCES model applied in this study covers the upper portion of the Gulf to the north of 24°N, and extending from 98°W to 82°W (Fig. 2). The model resolution is 70 sigma layers in the vertical and 5 km in the horizontal. Open boundaries were defined along the southern and eastern edges of the domain. Physical variables (temperature, salinity, currents, and sea surface elevation) were nudged every three hours using data from the HYCOM-NCODA analysis system (Cummings and Smedstad, 2013). Fourteen biogeochemical variables, including nutrients (nitrate, ammonium, phosphate, silicate, and iron), phytoplankton and zooplankton concentrations for different groups, dissolved organic and inorganic carbon, alkalinity, and calcite concentration, were provided as monthly climatological by MOM6-COBALT-NWA12, a 1/12 degree model for marine applications in the Northwest Atlantic (Ross et al., 2023).

Atmospheric forcing was obtained from the Navy Global Environmental Model (NAVGEM), consistent with the forcing used in the HYCOM NCODA analysis system. The background atmospheric pCO_2 was prescribed at 402 ppm, assuming negligible influence from rising atmospheric CO_2 over the simulation period. Dust and nutrient deposition were not considered, as atmospheric inputs are not major nutrient sources in this region (Kim et al., 2020).

A total of 23 rivers in the Northern Gulf were included in the simulation (Fig. 2). Discharge data were obtained from the U.S. Geological Survey (USGS) and the U.S. Army Corps of Engineers (USACE) at three-hour intervals. All river discharges were imposed as southward volume fluxes from the northern edge of grid cells near river mouths following the "active river" approach described by Sun et al. (2022). Biogeochemical tracers in each river, including nitrate, ammonium, phosphate, silicate, dissolved organic carbon, dissolved inorganic carbon, dissolved oxygen, and alkalinity, were primarily derived from the RC4USCOAST dataset, using monthly climatological values averaged over the period from 1990 to 2020 (Gomez et al., 2023). For missing values in the dataset, literature sources and USGS station data were

used as supplemental inputs (Kaushal et al., 2013).

The initial physical fields were obtained from Sun et al. (2022), and the biogeochemical variables were sourced from the MOM6-COBALT-NWA12 climatology. The model was spun up using repeated 2016 forcing until the biogeochemical fields reached a stationary state. The year 2016 was selected for spin-up because its mesoscale dynamics and Loop Current behavior are close to the climatological patterns. Following the spin-up, simulations were conducted for 2017 and 2018. Previous studies have validated the physical performance of CROCO simulations in nearly identical configurations by comparing modeled water temperature, salinity, and current features with observations (Liu et al., 2021; Lopera et al., 2025). Further model calibration and validation specifically for the biogeochemical fields over all three years can be found in Appendix A. In general, our model successfully captures the main horizontal and vertical spatial patterns, as well as seasonal variability in chlorophyll concentrations, net primary production, concentrations of alkalinity and DIC, and surface pCO_2 when compared with satellite, ship-based, and in-situ measurements. Although some data-model misfits remain, such as relatively poor performance in reproducing biogeochemical tracers along the coast of Florida, overall our results indicate that the model performance should capture the main dynamics and primary differences between different AE and EW scenarios.

2.3 Alkalinity modification simulations

We designed eight large scale river-based alkalinity modification scenarios (Table 1). All experiments focus on the consequences of increasing total alkalinity concentrations and for some of them DIC concentrations as well in the discharge from the Mississippi and Atchafalaya Rivers. These two rivers are the largest in the region and contribute the majority of freshwater and nutrient inputs to the Northern Gulf (Fig. 3b).

Four scenarios simulate AE, in which only concentrations of alkalinity (ALK) were increased in the river discharge. The remaining four scenarios represent a simplified form of EW, in which both alkalinity and an equivalent amount of DIC were added to river discharge at a 1:1 ratio (Kanzaki et al., 2023). For both the AE and EW scenarios, we considered four modification strategies to evaluate how different input magnitudes and timings influence the efficiency of these interventions. First, we applied a 10% increase in riverine ALK (or ALK+DIC) concentrations sustained throughout the entire model year 2017 (hereafter, Year10%). Second, we introduced a one-month pulse that doubled the concentrations in January 2017 (hereafter, Jan100%). Third, we applied a one-month pulse with a 10% increase in January 2017 (hereafter, Jan10%). Forth, we applied the same total amount of alkalinity and DIC as in the third strategy but distributed it to river loadings beginning on May 12, 2017, at a time of high river discharge (Fig. 3b) and shallow surface mixed layer in the Northern Gulf (hereafter, MayEqJan10%).

The interventions in the first and second strategies result in estimated total additions of 1.37×10^{11} mol and 1.065×10^{11} mol of alkalinity and DIC, respectively. These amounts are consistent with those used in other alkalinity enhancement studies, including the global estimates by Zhou et al. (2025), which applied additions of 2×10^{11} mol and 6×10^{11} mol per ocean patch, Liu et al. (2025) with 1.34×10^{11} mol in the North Sea, and Ou et al. (2025) with 1.03×10^{11} mol applied as in our case to the Northern Gulf. The third and fourth strategies involve a smaller addition of 1.065×10^{10} mol, which may be more easily attainable

in regional deployments.

Table 1. Summary of alkalinity modification scenarios.

River modifications	AE	EW
Control run	-	-
10% increase in 2017 (Year10%)	1.37×10^{11} mol extra ALK added through 2017	1.37×10^{11} mol extra ALK + equivalent DIC through 2017
100% increase in Jan (Jan100%)	1.065×10^{11} mol extra ALK added through 2017 January	1.37×10^{11} mol extra ALK added through 2017 January
10% increase in Jan (Jan10%)	1.065×10^{10}mol extra ALK added through 2017 January	1.065×10^{10} mol extra ALK added through 2017 January
10% increase (of Jan) in mid-May (MayEqJan10%)	1.065×10^{10} mol extra ALK added through 2017 May	1.065×10^{10} mol extra ALK added through 2017 May

In addition to the alkalinity modification scenarios, we conducted a simulation that continuously released passive tracers from the Mississippi and Atchafalaya Rivers during 2017–2018 to diagnose the spatial and temporal variability associated with physical advection and mixing.

2.4 Calculation of CO_2 uptake efficiency

CO_2 uptake efficiency η is originally defined as a dimensionless number equal to the ratio of the DIC inventory change to the cumulative added alkalinity (Eq. 1):

$$\eta = \frac{\Delta DIC(t)V}{\Delta ALK_{river}(t)} \quad (1)$$

where $\Delta DIC(t)$ is the difference in the spatially (volume-weighted) average of DIC concentration between a scenario run and a control run over time, summed across the simulated domain ($mol\ C/m^3$), V is the domain volume (m^3), and $\Delta ALK_{river}(t)$ is the cumulative riverine alkalinity addition ($mol\ eq$).

However, the definition in Equation 1 is not suitable for our study for two reasons. First, our model is a regional model and the model domain has an open-boundary system, such that DIC exchange across the open boundary complicates the attribution of cumulative DIC changes solely to atmospheric CO_2 uptake (Fig. S1). Since the perturbation is applied to the Northern Gulf coast, and the simulation is only run for <2 years, air-sea carbon exchange outside of the regional model domain is negligible on relatively short timescales. Second, in EW scenarios, there is additional DIC introduced through river inputs, which complicates the attribution of the simulated DIC change to air-sea CO_2 exchange. The uptake efficiency can be measured focusing on the changes in air-sea carbon exchange rather than the DIC inventory change. Therefore, we modified Equation 1 by replacing the volume-integrated DIC change with the integrated air–sea CO_2 flux over time and surface area, allowing for a more direct quantification of DIC changes from the drawdown of atmospheric CO_2 alone. This leads to Equation 2:

$$\eta = \frac{A\int_0^t \Delta F(t)}{\Delta ALK_{river}(t)} \quad (2)$$

where $\Delta F(t)$ is the difference in the spatially (area-weighted) average of air–sea CO_2 flux between scenario runs and control run over time ($mol\ C/m^2$/day), integrated over the simulation period and A is the surface area of the model domain (m^2).

In addition to integrating $\Delta F(t)$ over the simulation period to calculate η, we also defined a daily η (η_{day}) contribution, expressed as the instantaneous ratio of oceanic CO_2 uptake, $A\Delta F(t)$, to the total alkalinity added to the river (Eq. 3). Summing the daily contributions recovers the overall η value given in Eq. 2. Therefore, η_{day} reflects the short-term (daily-scale) efficiency in driving air–sea CO_2 exchange in units of day^{-1}. To ensure comparability across different modification scenarios and to minimize noise from variability in continuous riverine inputs during the addition period, we use the total amount of alkalinity ($\Delta ALK_{river,total}$) added to the river rather than the time-dependent $\Delta ALK_{river}(t)$ in the denominator of Equation 3.

$$\eta_{day} = \frac{A\Delta F(t)}{\Delta ALK_{river,total}} \quad (3)$$

2.5 Process attribution of air-sea CO2 exchange

Ito and Reinhard (2025, hereafter IR25) proposed a new framework for attributing air–sea carbon fluxes to specific physical and biogeochemical processes. Briefly, this approach combines carbonate chemistry, surface carbon budget and gas exchange parameterization to express the evolution of air-sea CO_2 exchange as a first-order ordinary differential equation.

$$\frac{dF}{dt} = -\lambda F + \sum_n f_n \quad (4)$$

where λ is the inverse of the air-sea CO_2 exchange timescale, and f_n are the forcing from physical and biogeochemical processes contributing to air–sea CO_2 exchange (e.g., advection, mixing, biological uptake, changes in temperature, salinity, alkalinity, atmospheric CO_2, and gas exchange). Mathematical derivation and formulation of Eq (4) can be found in IR25. This approach has proven effective in both an idealized two-box nutrient–carbon cycle model and a three-dimensional simulation of an iron and alkalinity release in the Southern Ocean. Here, we applied the same framework to our study. The key concept of this framework is that air–sea CO_2 flux integrates the effect of individual forcings over the CO_2 exchange timescale as expressed as the negative feedback term (Eq. 4). The timescale is set by G, the air-sea gas exchange coefficient (*m/day*), expressed as a function of wind speed and the Schmidt number for CO_2 (Wanninkhof, 2014), α_C, a dimensionless carbonate chemistry coefficient that reflects the sensitivity of surface pCO_2 to perturbations in DIC, and *h*, the surface mixed layer depth (m).

$$\lambda = \frac{G\alpha_C}{h} \quad (5)$$

where λ has unit of day^{-1} and represents the strength of the negative feedback by which air–sea CO_2 flux drives the surface ocean back toward equilibrium after a disturbance induced by an external forcing. In other words, the larger the value of λ, the faster the surface ocean returns to equilibrium following a perturbation. *G* and *h* can vary due to atmospheric wind and ocean mixed layer variability, and their

climatological mean values are used for the calculation of the representative λ value. We applied this framework to the Northern Gulf by integrating over the full simulation period and focusing on the upper 10 meters of the water column, representing the annually averaged mixed layer depth estimated through a regression-based diagnostic approach using model outputted sea surface temperature time series. Advection and mixing terms were obtained directly from the model's DIC diagnostic equation. Temperature, salinity, and alkalinity were extracted from the standard model output. Values for the biological carbon sink, atmospheric CO_2, and gas transfer coefficient were obtained by modifying the model code to output these non-standard output variables. Eq. (4) is numerically integrated using Euler forward time-stepping scheme, and sensitivity tests with the fourth-order Runge–Kutta method confirmed the robustness of the numerical calculation.

3.Results

3.1 Natural seasonal and spatial variability

To provide context on the Gulf's baseline conditions prior to any alkalinity modification, we present the two-year monthly averaged spatial distributions of air–sea CO_2 flux and passive tracer concentrations from the control run (Fig. 4). The air–sea CO_2 flux highlights the natural variability in CO_2 exchange across the region, and the passive tracers reveal the transport pathways that added alkalinity or DIC from riverine sources will be subject to.

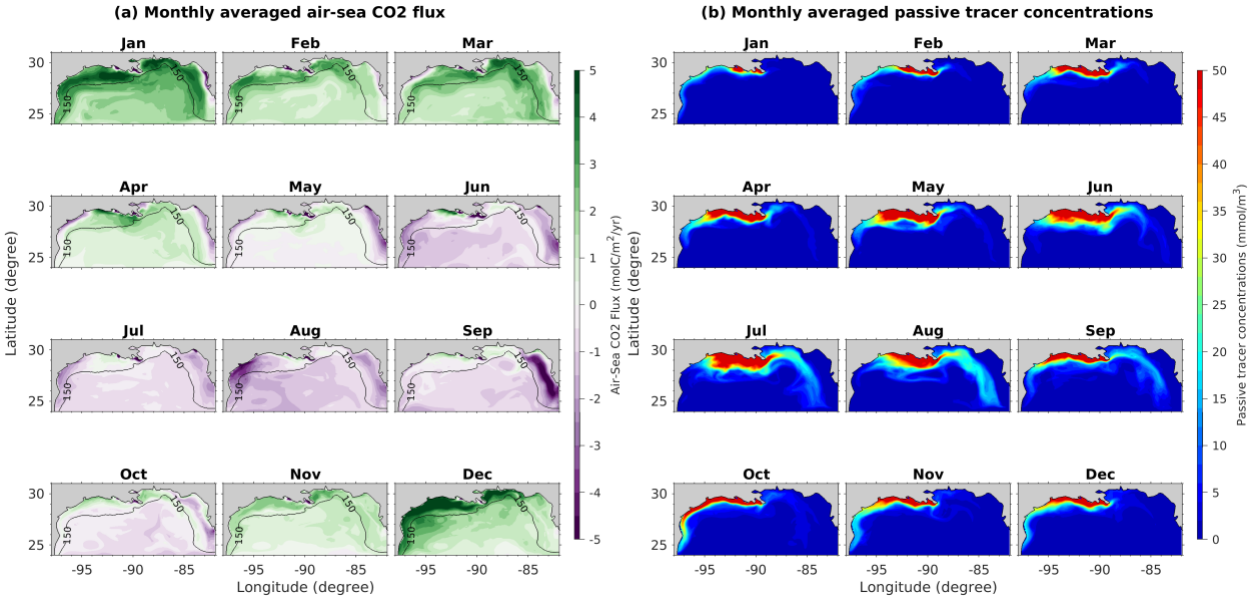

Fig. 4 Two-year monthly averaged spatial distributions of air–sea CO_2 flux (a) and passive tracer concentrations (b) from the control run. Positive values denote CO_2 fluxes from the atmosphere into the surface ocean.

Figure 4a shows that the Northern Gulf acts as an ingassing system during winter and spring, absorbing CO_2 from the atmosphere, and transitions to outgassing in summer and fall when surface waters are warmer. These seasonal changes are stronger in nearshore regions, following the spatial pattern of high chlorophyll concentrations where the biological pump consumes DIC (Fig. A3). Most of the CO_2 uptake

occurs along the Northern Gulf coastline in winter, whereas peak outgassing is simulated along the Florida coast in summer. However, this pronounced summer outgassing along the Florida coast may reflect in part a numerical artifact, as satellite observations do not indicate high chlorophyll concentrations during that season (Fig. A3).

Figure 4b shows that passive tracers released from the Mississippi and Atchafalaya Rivers are generally carried westward along the shoreline by surface currents driven by predominantly east-to-west winds. During summer (June–September), part of the plume is transported east of the Mississippi Delta as currents reverse under weakened winds, eventually interacting with the Loop Current system and spreading offshore into the open Gulf. This result suggests that under the proposed alkalinity modification scenarios additional air–sea CO_2 exchange is most likely to occur along the Texas–Louisiana coastline, with the strongest signals near the Mississippi Delta, rather than in the eastern Gulf.

3.2 Distribution of added alkalinity

The temporal and spatial distribution of added alkalinity and DIC in the surface ocean is critical for determining when and where CO_2 uptake occurs and how efficient it is, since only surface-retained additions contribute to air–sea exchange. We present the surface footprint of added alkalinity for the three one-month AE pulse scenarios in Figure 5. Alkalinity is emphasized here because surface DIC is influenced by both river inputs and air–sea CO_2 exchange, whereas alkalinity is not affected by the air-sea CO_2 exchange and primarily governed by hydrodynamics.

The Jan100% scenario forms the largest surface alkalinity plume due to the greater riverine input. During the month of addition, most alkalinity remains near the Mississippi Delta, with stronger accumulation west of the delta rather than to the east. By the following month, it is advected eastward by wind-driven currents and entrained into the Loop Current, propagating southeastward into the open Gulf. The Jan10% scenario produces a similar spatial pattern, as alkalinity is also added in January. In comparison, the MayEqJan10% scenario spreads alkalinity over a broader region and retains it closer to the surface due to higher river discharge and shallower mixed layer. By the following month, most additions are transported west of the Delta, consistent with the passive tracer result.

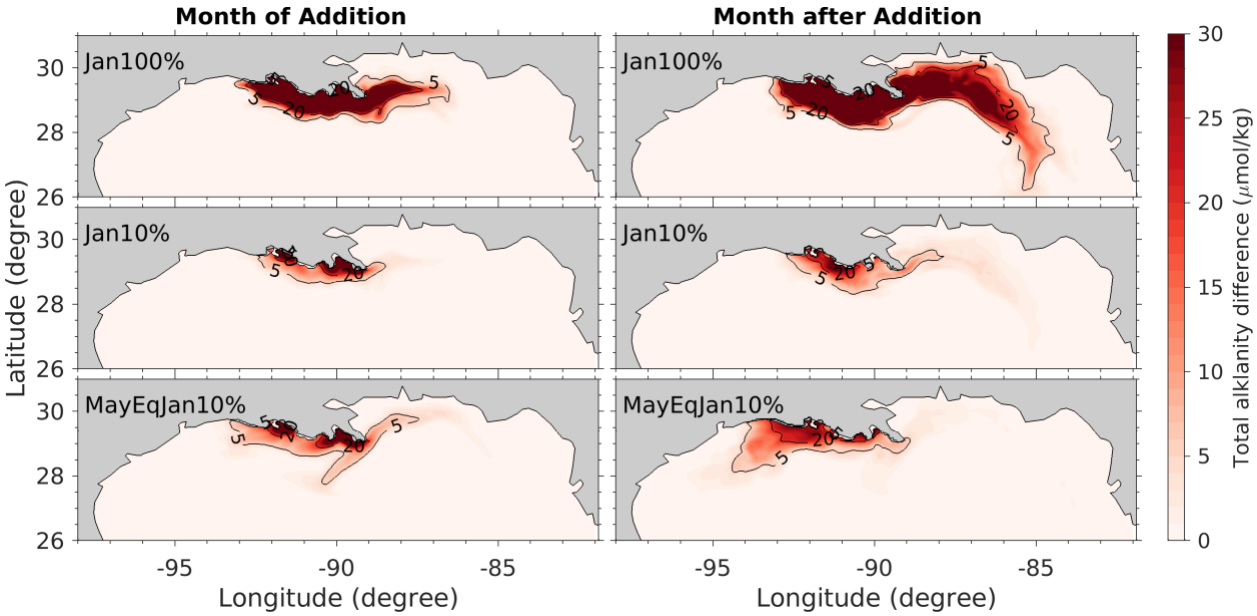

Fig. 5 Surface footprint of added alkalinity for the one-month AE pulse scenarios, represented as differences in average alkalinity concentrations in the upper 10 m between each scenario and the control run. Results are shown as monthly averages for the month of addition (left) and the subsequent month after the addition stopped (right). The EW scenarios (not shown) exhibit surface similar footprints.

Figure 6 shows the amount of added alkalinity retained in the upper 10 m, which directly contributes to air–sea CO_2 exchange, expressed as both total inventory and percentage of riverine addition. The Jan100% scenario shows the highest retention inventory, peaking at about 7×10^{10} mol by the end of the one-month addition before declining as alkalinity is redistributed to deeper layers. The two 10% one-month pulse scenarios follow a similar temporal pattern, with peak retention inventories about one seventh of the 100% scenario.

The percentage results provide a different perspective. Among the one-month pulse scenarios, the MayEqJan10% scenario shows much higher retention than the two January additions, particularly between days 50 and 100. The two January scenarios yield nearly identical retention, as they are subject to the same winter–spring conditions.

The added alkalinity in the MayEqJan10% scenario shows high retention, benefiting from both elevated river discharge and a shallow mixed layer. To disentangle these two effects, we conducted a sensitivity experiment in which the river discharge from January 2017 was shifted to begin in May 2017, and the 10% one-month addition was repeated based on this modified run. The results show only minor differences between the control and sensitivity runs (green solid versus green dashed lines), indicating that changes in mixed layer depth are the primary factor determining the higher retention of the MayEqJan10% scenario.

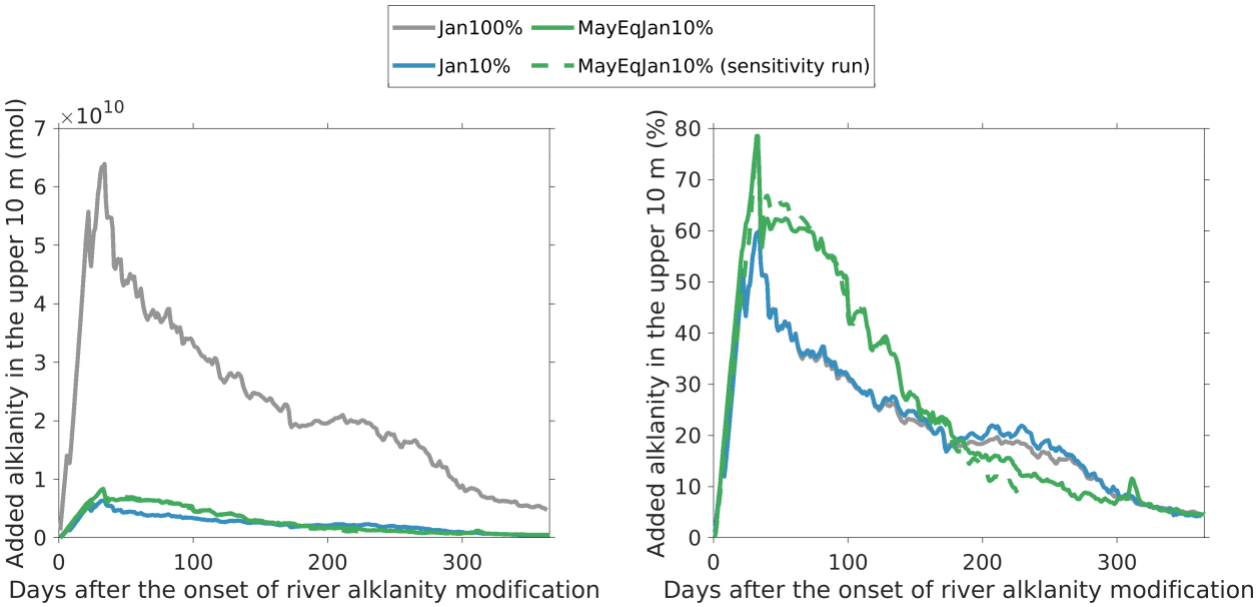

Fig. 6. Added alkalinity summed across the entire model domain and within the upper 10 m, shown as total inventory (left panel) and as the percentage of riverine additions (right panel).

3.3 CO_2 uptake efficiency

Figure 7 presents the temporal evolution of CO_2 uptake efficiency across all alkalinity modification scenarios. In AE scenarios, η increased rapidly during the first 7–8 months before stabilizing with only minor changes, reflecting the timescale for the air-sea CO_2 transfer to fully respond to the added alkalinity. Final η values varied, with the Jan100% scenario yielding the lowest value (0.58). Reducing the addition to 10% in the same month increased η to 0.76, and similarly the Year10% scenario produced an efficiency of 0.72. These results suggest that smaller modifications in river alkalinity concentrations lead to higher η. This does not include the potential inorganic precipitation of calcium carbonate particles in the case of strong alkalinity increase (Jan100%), thus the efficiency of 0.58 should be considered as an upper bound (Fig. S2). The timing of addition also matters. The summer alkalinity release scenario (MayEqJan10%) reached an η of 0.85, considerably higher than the equivalent winter case (Jan10%). The higher summer efficiency coincided with both a shallower mixed-layer and with the transition towards seasonal outgassing.

All EW scenarios produced small but negative η values, indicating that introducing both ALK and DIC in a 1:1 ratio result in CO_2 release to the atmosphere, through an ocean-side "carbon leakage" (e.g., Kanzaki et al., 2023). In the EW cases, η did not converge to a steady state but fluctuated within a relatively small absolute range. Final values differed only slightly, ranging between –0.12 and –0.15 (Fig. 7). A slight "leakage overshoot" was observed in the summer release scenario at the end of 2017, which was subsequently mitigated in early 2018 due to the influence of strong winter mixing due to high winds. These dynamics reflect the fact that for a given perturbation to marine ALK concentrations the EW case introduces DIC at a relative excess to background dissolved pCO_2, but at a smaller deviation overall from the background ALK/DIC field (see Section 4.1). In addition, this implies that for a given alkalinity introduction the ultimate quantity of carbon storage will be larger for the EW case than for the AE case (Fig. 7).

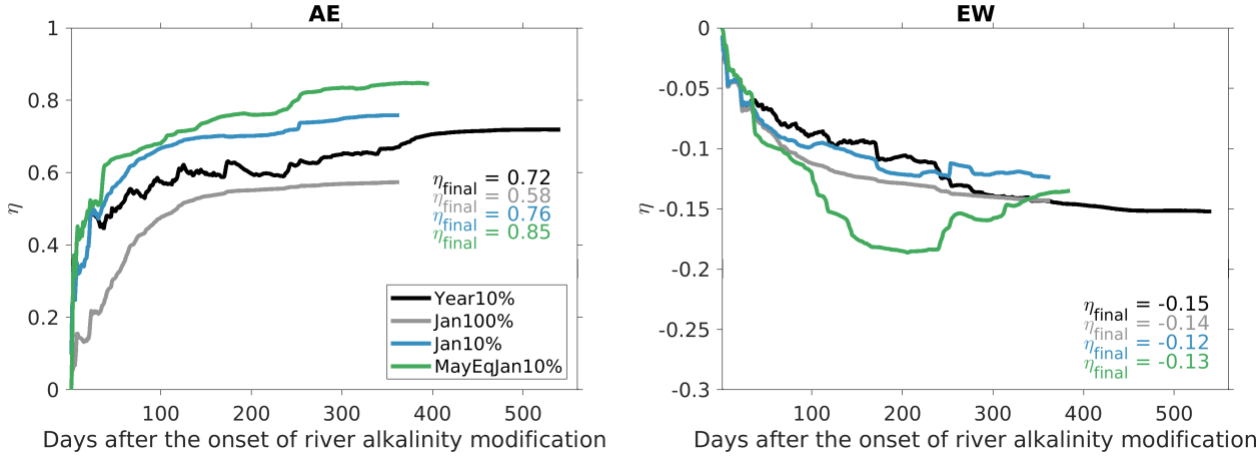

Fig. 7. The CO_2 uptake efficiency (η) for different AE (left) and EW (right) scenarios. The accumulated CO_2 uptake used to calculate η is the sum over the entire model domain. η_{final} indicates the η values for the different scenarios at the end of the simulations. The three one-month addition cases are simulated for about one year, as η changes only minimally after that period. The Year10% case runs for more than 500 days because alkalinity is continuously added throughout an entire year, followed by an extended simulation to capture η changes beyond that period.

3.4 Air–Sea CO_2 flux

Besides surface retention of added alkalinity or DIC, temporal variations in the rate of air–sea CO_2 gas exchange influence uptake efficiency. A higher exchange rate reduces the chance that the alkalinity or DIC retained near the surface is advected to the deep ocean. Figure 8 shows Northern Gulf-integrated differences in air–sea CO_2 flux between modification scenarios and the control run, along with corresponding η_{day} contributions. The flux represents the total amount of CO_2 absorbed in the Northern Gulf, and η_{day} reflects changes in the efficiency of absorption.

In the AE scenarios, one-month pulses follow similar temporal patterns, with flux peaking near the end of the modification period and gradually declining toward equilibrium afterward. Later, when vertical mixing in the ocean was enhanced by occasional hurricanes or by seasonally intensified winter mixing in the following year, the river-derived alkalinity that had been transported to subsurface layers was brought back to the surface, leading to several minor episodes of CO_2 uptake (e.g., day 250). The Jan100% scenario produces the largest flux and the longest recovery time, reflecting the stronger chemical disequilibrium it induces. The Jan10% and MayEqJan10% scenarios show comparable but smaller fluxes, with the January scenario recovering more slowly. η_{day} contributions, however, diverge from the flux patterns. The Jan100% scenario, despite yielding the highest flux, produces the lowest η_{day} during and after modification, consistent with its prolonged recovery time. The Jan10% and MayEqJan10% scenarios achieve similar peak efficiencies, but the May addition sustains a broader window of high efficiency during the first 50 days.

The difference between the Jan100% and Jan10% scenarios can be attributed to the α_C term in Eq. 5. A larger river alkalinity input pushes the system farther from equilibrium, which reduces the sensitivity of

CO_2 uptake per unit alkalinity added. The slight increase from Jan10% to MayEqJan10% is because of the shallower mixed layer in summer compared with winter.

The EW scenarios reproduce the AE pattern of air–sea CO_2 flux but with negative values (outgassing) and much smaller magnitudes. For example, in the Jan100% case, the peak flux is ~3.8×10^8 mol C/day, about one third of the corresponding AE value (1.2×10^9 mol C/day). Moreover, similar subsequent minor episodes of air–sea CO_2 exchange occurred in the EW cases as well, appearing as either uptake or outgassing depending on the ratio of river-derived DIC and ALK that were mixed back into the surface layer. Daily contributions to the efficiency are nearly identical in the Jan100% and Jan10% cases, while the MayEqJan10% simulation is characterized by a lagged peak and stronger fluctuations. However, these variations in η_{day} are small (on the order of 10^{-3}), and overall differences among the efficiencies in the EW scenarios negligible.

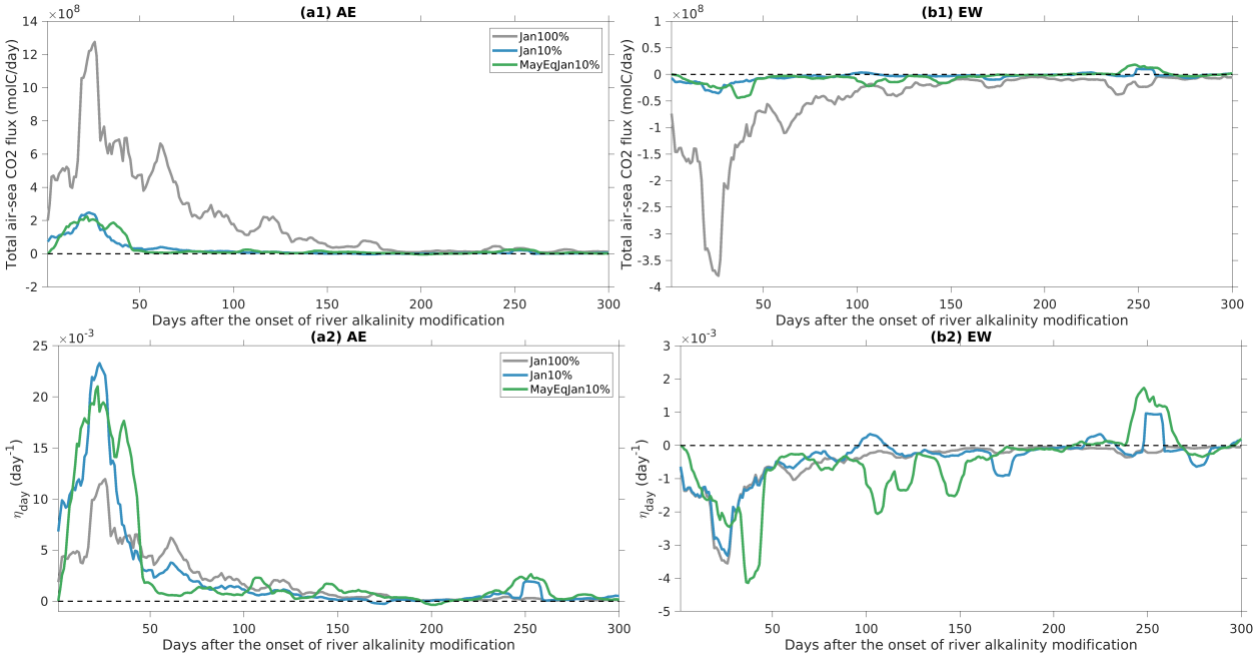

Fig. 8. Upper panels: daily domain-summed air–sea CO_2 flux differences between the control run and the AE (a1) and EW (b1) scenarios. Lower panels: η_{day} contributions from the corresponding AE (a2) and EW (b2) scenarios. The black dashed line represents the zero baseline.

3.5 Attribution of air–sea CO_2 flux changes

The mechanisms driving the air-sea carbon fluxes in both AE and EW scenarios are highlighted in Figure 9. We selected the Jan100% case, because it induces the largest disequilibrium and produces the clearest anomaly signals above background variability. Dynamic patterns of air–sea CO_2 exchange, however, are consistent across AE and EW scenarios, with a representative exchange timescale (λ^{-1}) of approximately 58 days. Full air-sea equilibration takes 2-3 times this e-folding timescale, consistent with the evolution of air-sea CO_2 flux in Fig. 8.

In the AE simulations, adding alkalinity promotes atmospheric CO_2 uptake at the surface, enhanced by wind-driven exchange. Physical transport and mixing simultaneously dilute newly formed DIC,

sustaining active uptake. Once the addition is stopped, dilution of surface alkalinity creates localized reductions that can trigger sea-to-air outgassing. This process, however, is largely offset by the redistribution of absorbed DIC, allowing fluxes to return toward equilibrium.

In the EW case, the dynamics differ because rivers also supply additional DIC, which appears in the transport term. The imbalance between the added DIC and ALK leads to net outgassing in the first month, further amplified by wind. Once additions cease, transport and mixing dilute both DIC and ALK, returning air–sea fluxes toward equilibrium, as in the AE case.

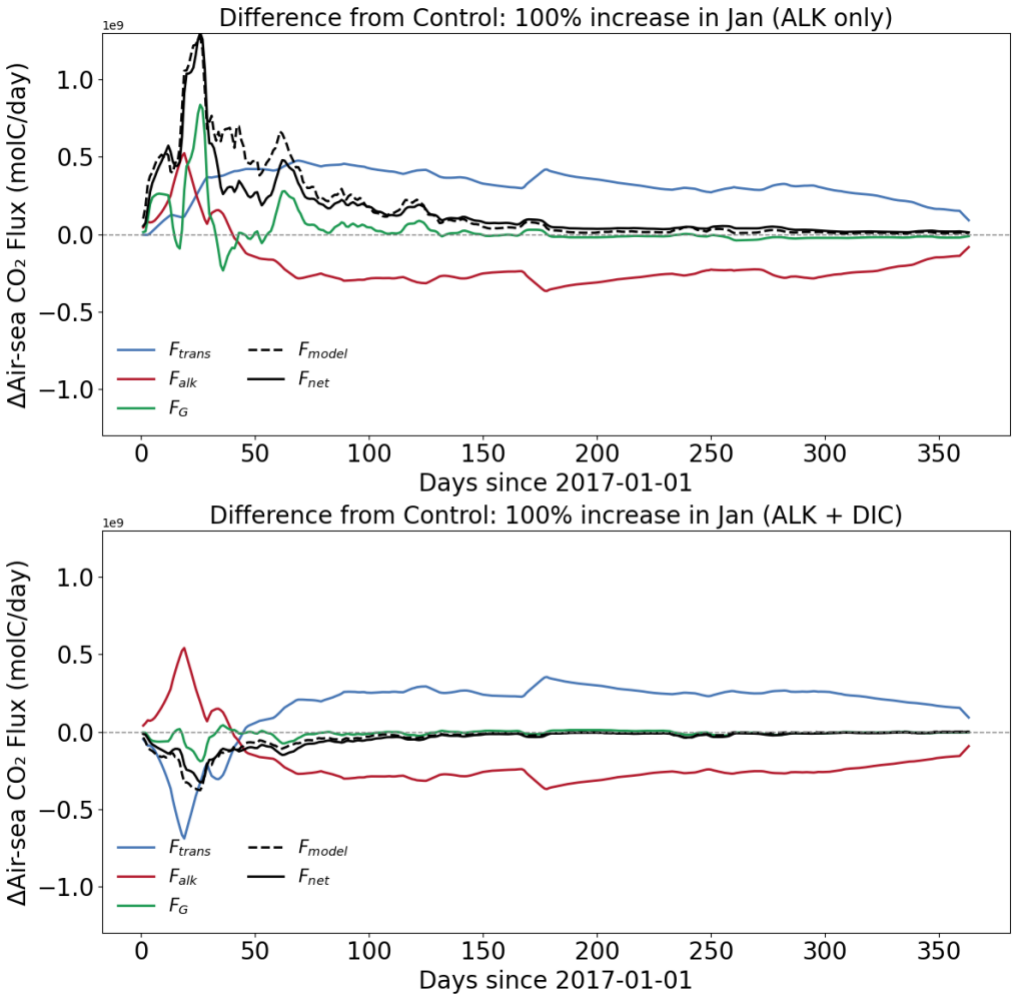

Fig. 9. Attribution of air-sea CO_2 flux anomalies for the 2017-Jan100% scenario in AE and EW. Anomalies are integrated over the entire model domain, with positive values indicating fluxes into the ocean. Only the dominant drivers identified by the attribution framework, accounting for 99% of the fluxes, are shown.

4.Discussion

4.1 A framework for explaining efficiency changes across modification scenarios

A simple framework in DIC/ALK space can help explain how η varies under different modification pathways. In Figure 10, we show equilibrium $CO_{2(aq)}$ contours calculated with CO2SYS at T = 25 °C and

S = 35.5 psu using a range of DIC and alkalinity combinations. The black dot marks the background ocean state, and the dotted line shows the background DIC/ALK ratio (0.87), which is closely aligned with the equilibrium $CO_{2(aq)}$ contours. Although this ratio varies seasonally and regionally in the Northern Gulf (0.85–0.90), a single reference is used for clarity. The yellow and pink lines represent the AE and EW pathways, respectively.

Post-perturbation, DIC/ALK values asymptotically approach the background ratio via a non-linear trajectory. If the air–sea CO_2 exchange was the only process at play (e.g., neglecting ocean dynamics), the trajectories would follow the vertical pink and yellow arrows in Fig. 10 until they intersect the background line. These intersections mark the maximum potential CO_2 uptake for AE and the maximum potential CO_2 loss for EW, respectively. The corresponding efficiency is given by

$$\eta_{max} = -\frac{DIC_{modification}}{ALK_{modification}} + \frac{DIC_{background}}{ALK_{background}} \quad (6)$$

Where the η_{max} represents the difference between the DIC/ALK ratio ($\frac{DIC_{modification}}{ALK_{modification}}$) imposed by the alkalinity modification and the background ocean DIC/ALK ratio ($\frac{DIC_{background}}{ALK_{background}}$). In the AE scenario the modification ratio equals 0, so η_{max} is determined by the background ratio (0.87). In the EW scenario, the modification ratio equals one, which gives η_{max} = - 0.13. All simulated η values in Section 3.3 for AE scenarios are smaller than this theoretical maximum, and the values from EW scenarios are around the theoretical maximum.

In reality, ocean dynamics impact efficiency. For AE, transport and mixing redistribute added alkalinity from the surface to depth, and this contribution is represented as a retreat along the yellow trajectory, with the vertical offset from the background line representing the realized CO_2 uptake. This retreat lowers realized η relative to η_{max}, as shown by the white arrow. Stronger winter mixing compared to summer mixing enhances alkalinity loss (a greater retreat), causing η from the Jan10% scenario to be smaller than the MayEqJan10% scenario. In addition, in the Jan100% scenario a slow air–sea exchange prolongs equilibration, allowing more time for ocean advection to redistribute alkalinity to depth, further reducing η.

In the EW scenarios, physical transport and mixing contribute to the removal of both DIC and ALK from the mixed layer. This is represented as a retreat along the pink trajectory, with the vertical offset from the background line indicating the total amount of CO_2 loss. However, this contribution is difficult to quantify in the simulated η values because the EW perturbations are small relative to the background ALK/DIC field and equilibrate rapidly in the shallow coastal regions where outgassing occurs. As a result, most simulated values remain close to the theoretical maximum. This is a key contrast between AE and EW — stronger physical transport and mixing reduce the effectiveness of AE, but increase the relative effectiveness of EW, with respect to ocean carbon storage.

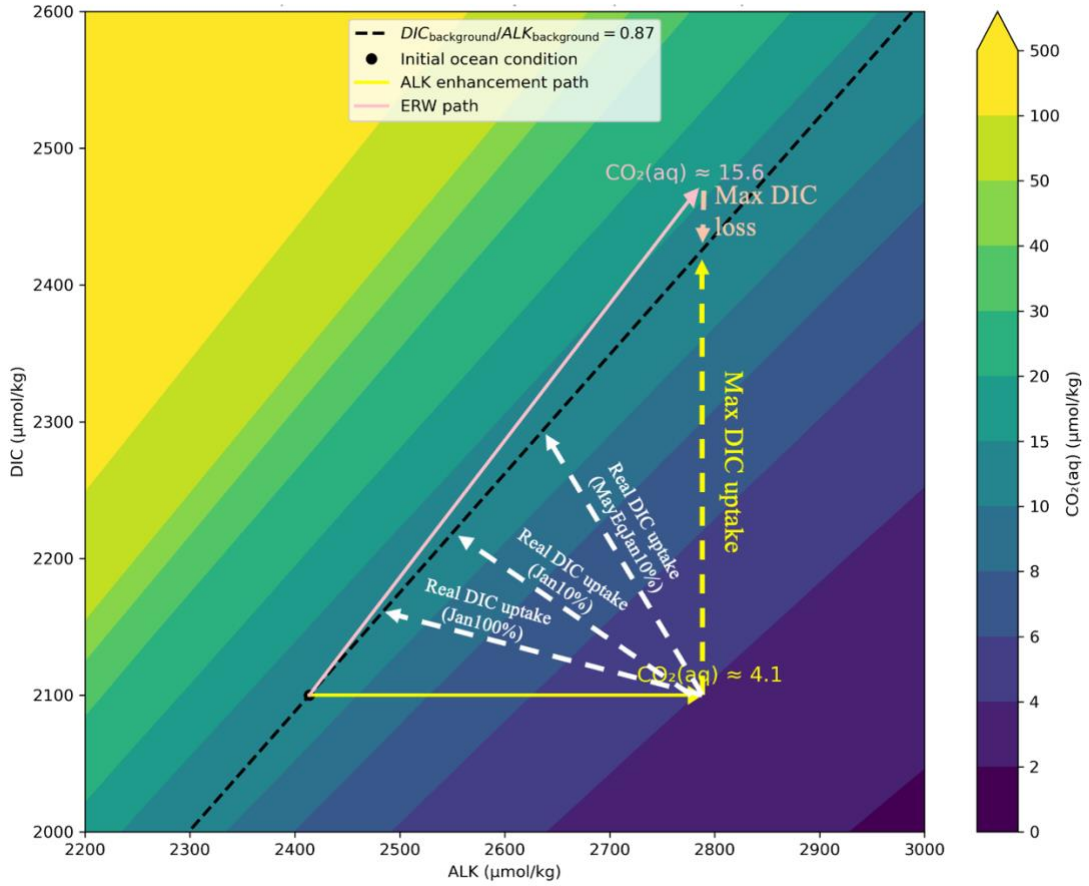

Fig. 10. Conceptual diagram showing how η varies across different alkalinity modification scenarios in the DIC/alkalinity space. Arrows represent conceptual directions, and do not reflect the actual results of the simulations.

4.2 η in the Northern Gulf across the literature

The simulated η values for the AE scenarios in this work range from 0.58 to 0.85. This range encloses the Gulf-wide efficiency of 0.6–0.7 reported by an independent study using one-month alkalinity pulses across globally distributed ocean patches (Zhou et al., 2025). Ou et al. (2025) simulated river-sourced alkalinity enhancement scenarios in the Gulf by increasing river alkalinity by 10% during 2021–2022, with a total addition of 1.03×10^{11} mol, comparable to our Year10% scenario (1.065×10^{11} mol). Despite similar amounts added, their simulated a CO_2 uptake (~4.09×10^{10} mol, η = 0.4) is substantially lower than ours (~9.9×10^{10} mol, η = 0.72). This difference may be attributed in part to model resolution. Their 1 km model permits submesoscale dynamics, which enhance vertical transport, reducing the retention of added alkalinity in surface waters and lowering η. Their framework also showed strong CO_2 outgassing in the open Gulf, which was not captured in our simulation. This discrepancy may also stem from structural differences between their biogeochemical module and parameterization choices, as well as sensitivity to hydrodynamic variability at fine scales.

Comparisons with OAE experiments in other parts of the word indicate that, with an appropriately designed strategy, η can exceed 0.70, as found for the North Sea and northern Brazil (η > 0.7; He and

Tyka, 2023; Liu et al., 2025). These regions share an upper ocean stratification that favors alkalinity retention in the mixed layer for long enough to sustain air–sea CO_2 exchange. Some open-ocean regions report even higher efficiencies, reaching 0.96 in the Bering Sea (Wang et al., 2023) and above 0.8 in the Southern Ocean (Burt et al., 2021). However, coastal or river-based enhancement strategies retain significant cost and operational advantages against dispersing large quantities of alkaline material offshore. AE when performed at river mouths has an added benefit of the discharge naturally spreading alkalinity, expanding the area available for CO_2 uptake.

For the EW case, our simulations suggest that approximately 12–15% of the CO_2 drawdown through land-based strategies is subsequently released back to the atmosphere from the ocean, independently of the details of the discharge. Although there are fewer existing estimates of ocean-side CO_2 leakage (Kanzaki et al., 2023; Beerling et al., 2025a), our results are generally consistent with existing work indicating that ocean CO_2 leakage is a relatively small component of the overall EW life cycle (e.g., at or below ~10-15% for silicate feedstocks and ~20-30% for carbonate feedstocks). However, it will be important to further refine these estimates at additional locations and with higher resolution ocean models that include a fully comprehensive ocean-sediment carbonate system.

4.3 Planning perspective

Our simulations show that small additions of alkalinity to riverine discharge yield higher CO_2 uptake efficiency than large perturbations. Strategies that sustain modest increases in alkalinity over longer periods are therefore likely to be more efficient than short, concentrated pulses (e.g., Year10% vs. Jan100%). In the Northern Gulf, alkalinity enhancement is also more effective in summer than in winter because a stronger stratification and shallower mixed layer promote a longer surface retention of the added alkalinity (e.g., MayEqJan10% vs. Jan10%).

While smaller perturbations maximize efficiency, they may not achieve the total CO_2 uptake needed for large-scale mitigation. In our simulations, one-month 10% additions produced about $8–9 \times 10^9$ mol of uptake, about an order of magnitude less than the more expensive Jan100% scenario or Year10% scenarios, highlighting a trade-off between efficiency, total carbon removal, and implementation costs. Cost-effective strategies would favor smaller additions, whereas maximizing sequestration would require accepting lower efficiency.

For EW cases, our simulations reveal only minor differences in the amount of ocean-side leakage, making it a less pressing concern for strategy design. Instead, effective approaches should focus on land-based factors such as mineral feedstock, weathering kinetics, cost, and signal resolvability (Paulo et al., 2021; Deng et al., 2023; Li et al., 2024; Suhrhoff et al., 2024; Beerling et al., 2025a, b, Kanzaki et al., 2025). In addition, our results imply that in general for a given amount of ALK modification, EW approaches will tend to result in more effective ocean carbon storage because they will tend to deviate less strongly from the background ALK/DIC field during transient ALK modification.

4.4 Limitations and future work

Limitations of this study are in the regional ocean model framework, the resolution of the ocean model, and the uncertainties related to the representation of the biogeochemical processes. The regional framework prevents tracers exiting the Northern Gulf from being tracked. This may cause an

underestimation of both amount and efficiency of CO_2 uptake in alkalinity enhancement scenarios, since alkalinity transported beyond the boundary is no longer represented, and could resurface elsewhere. However, most CO_2 uptake occurs within the first 100 to 150 days after addition (Fig. 6, Fig. S2). By the time the added alkalinity exits the Northern Gulf, the majority (about 80%) has already entered the subsurface layer. Consequently, any subsequent alkalinity mixing back to the surface, whether within the Northern Gulf or elsewhere, would contribute little compared with the uptake that occurs during the initial 4-5 months. Addressing this remaining uncertainty would require nesting the regional configuration within a global model to track the fate and potential resurfacing of exited alkalinity. In addition, we used a prescribed background atmospheric pCO_2 in this study, which we consider reasonable given the regional perturbations and the short, two-year simulation period. However, a fully coupled ocean–atmosphere system with a freely evolving pCO_2 field is required to accurately capture air–sea CO_2 exchange under larger and longer-term perturbations (Kanzaki et al., 2023; Tyka et al., 2025).

The horizontal resolution of our simulations (5 km) is insufficient to resolve submesoscale processes, which generally require grid spacing finer than 2 km. Submesoscale circulations alter biogeochemical tracer transport, especially in the vertical, (Liu et al., 2022), affecting air–sea CO_2 exchange. In the Northern Gulf, these processes modify freshwater plume spreading, deepen the mixed layer, and enhance vertical transport especially around mesoscale eddies (Luo et al., 2016; Liu et al., 2021, 2022). Higher-resolution simulations are needed to better constrain efficiency, but their computational costs, especially when coupled with a biogeochemical model, remain too high to allow the kind of scenario exploration performed in this work. In this regard, it is worth noting that while AE and EW are negative-emission approaches aimed at mitigating climate change, evaluating their feasibility through numerical simulations produces a substantial carbon footprint. Each of our one-year scenarios required ~30,720 CPU hours, equivalent to ~125.75 kg CO_2 emissions (Lannelongue et al., 2021; https://calculator.green-algorithms.org/). Finer resolution or a global investigation could increase this cost by an order of magnitude. A path forward may be represented by the development and adoption of AI-based emulators, which would enable a broad exploration of potential strategies at a lower carbon cost.

Lastly, in the PISCES framework, calcite precipitation is represented only through biologically mediated contributions to the biological pump. Specifically, calcite formation is driven through a specified ratio between particulate organic carbon (POC) and inorganic carbon (PIC) export and is then scaled to export production. However, abiotic calcite precipitation may occur if the saturation state (Ω) of calcite or aragonite is transiently driven to elevated values. In some cases, this may result in rapid, non-linear carbonate formation and in extreme cases could lead to net alkalinity export from the mixed layer (Hartmann et al., 2022; Moras et al., 2023). In our simulations, only a small area within the Mississippi Delta reached $\Omega_{calcite} > 7$, (Fig. S2), which indicates limited potential for abiotic calcite precipitation in our simulated perturbations. Abiotic precipitation will remove more alkalinity under a stronger pulse due to a greater increase in local alkalinity. Without the abiotic precipitation parameterization, a stronger pulse (Jan100%; η=0.58) is less efficient than a weaker one (Jan10%; η=0.76). While we suggest that modeling estimates of the effectiveness of ocean carbon storage through alkalinity modification should be standardized to include saturation-state dependent carbonate formation, we would not expect this to alter the primary results of this study, in particular that weaker pulses exhibit higher CO_2 uptake efficiency.

5.Conclusion

In this study, we applied a high-resolution regional ocean–biogeochemistry model to evaluate the effectiveness of two river-based alkalinity modification approaches (AE and EW) in the Northern Gulf of Mexico. We conducted eight hypothetical scenarios that varied the timing, magnitude, and duration of alkalinity and DIC additions in the Mississippi and Atchafalaya Rivers. Our analysis focused on the simulated amount and efficiency of CO_2 uptake or leakage for each strategy adopted, and the roles of ocean dynamics and air–sea fluxes in shaping the outcomes were examined. These results provide valuable guidance for designing carbon dioxide removal plans in the southern United States.

For the AE experiments, simulated CO_2 uptake efficiencies ranged from 0.58 to 0.85. Efficiency was higher for modest perturbations and for summer-time deployment. Smaller additions kept the system closer to the background equilibrium state, resulting in higher carbon uptake per alkalinity addition and greater integrated CO_2 uptake. In summer, warmer surface waters produced a shallower mixed layer, allowing more of the added alkalinity to remain near the surface and sustaining a broader window of high uptake efficiency.

For the EW experiments, the model results indicated that 12–15% of the carbon sequestered on land was re-emitted to the atmosphere from the ocean, largely independent of the timing or magnitude of the additions. This stable leakage from the ocean side can be explained by the relatively small perturbations of EW compared to AE. The EW simulations showed anomalies in air–sea CO_2 flux and η_{day} values that were an order of magnitude smaller than those in AE. As such, although the choice of strategy may still influence the percentage of leakage, the perturbation magnitude is so small that these differences are difficult to detect.

Lastly, we presented a simple framework in DIC–alkalinity space to explain efficiency differences across AE and EW scenarios. Theoretical efficiencies or leakages are determined by the initial DIC/alkalinity ratios in river inputs relative to the background ocean ratio, which in turn reflects the equilibrium carbonate chemistry. Ocean dynamics, through the vertical mixing of alkalinity, lower these theoretical values by redistributing added materials vertically, with part of the additions lost to the subsurface ocean before absorbing CO_2 from the atmosphere. Our results indicate that ocean dynamics exert a stronger influence on AE because of the larger perturbations in DIC–alkalinity space, necessitating explicit consideration of alkalinity loss to the ocean interior when developing AE strategies. In contrast, EW is less sensitive to ocean dynamics, and its effectiveness, life cycle assessment and sustainability potential should be assessed primarily in terms of land-based factors such as mineral feedstock and weathering processes.

Appendix A: Model validation and calibration

Observational data

Observational data from multiple sources were used to validate and calibrate the model. In situ measurements were obtained from two buoy stations located along the coastlines of Mississippi and Louisiana (Coastal MS and Coastal LA, Fig. A1), operated by the Pacific Marine Environmental Laboratory (PMEL) of the National Oceanic and Atmospheric Administration (NOAA). These stations provided continuous observations of sea surface temperature, salinity, and pCO2 for model comparison (https://www.pmel.noaa.gov/co2/story/Coastal+MS and

https://www.pmel.noaa.gov/co2/story/Coastal%20LA, accessed August 2025).

In addition to in situ observations, satellite-derived datasets were used to evaluate model-simulated chlorophyll concentration and net primary production (NPP). MODIS-AQUA provides 7-day mean chlorophyll data for the southeastern United States (https://erddap.marine.usf.edu/erddap/griddap/index.html?page=1&itemsPerPage=1000, accessed August 2025). The Oregon State University Ocean Productivity Lab provides global NPP estimates from multiple algorithms (MODIS-CBPM, MODIS-standard VGPM, VIIRS-CBPM, and VIIRS-standard VGPM) (https://orca.science.oregonstate.edu/npp_products.php, accessed August 2025).

Moreover, the *project: Collaborative Research: pH Dynamics and Interactive Effects of Multiple Processes in a River-Dominated Eutrophic Coastal Ocean* conducted multiple cruise-based measurements of dissolved inorganic carbon (DIC), total alkalinity (TA), pH, dissolved oxygen, and pCO2 in the Northern Gulf from 2017 to 2019, with cruise trajectories shown in Fig. A1. The TA and DIC data from these cruises were used to validate model simulations. All observations were obtained from the Biological and Chemical Oceanography Data Management Office (BCO-DMO) portal (https://www.bco-dmo.org/project/751332, accessed August 2025).

Finally, the SeaFlux product, a global 1° × 1° gridded dataset of pCO2 constructed using an ensemble approach that integrates six observation-based mapping products, was used to evaluate the model performance in simulating spatial patterns of pCO2 (Fay et al., 2021).

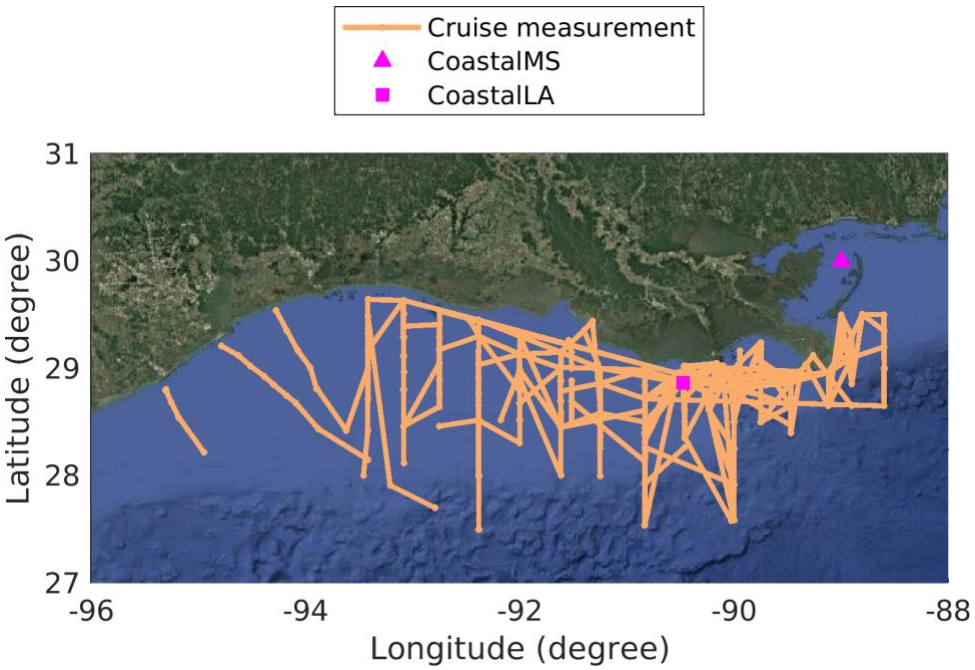

Fig. A1. Map showing the locations of in situ observations and the trajectories of cruise measurements.

Buoy-Based Observational Comparisons

Figure A2 compares sea surface temperature (SST), sea surface salinity (SSS), and pCO_2 between high-frequency buoy measurements and model outputs at two stations near the Mississippi Delta, both strongly

influenced by river discharge from Mississippi and Atchafalaya rivers. For SST, the model and observations show strong agreement for SST results at both stations (R>0.95), though the model underestimates values by ~1–1.5 °C, especially in spring when temperatures rise rapidly. Nonetheless, this level of agreement is encouraging, considering that the simulation is free-evolving, and the coarse-resolution model cannot capture complex submesoscale coastal processes.

For SSS, the comparison between the model and observations shows generally good agreement, with better consistency at Coastal LA than at Coastal MS. At Coastal MS, the model misses salinity decreases in May–June 2016 and 2017 because river salinity was prescribed as a fixed 4 PSU (Sun et al., 2022) to avoid numerical instability, preventing representation of temporal variability.

For pCO_2, the model captures the overall magnitude at both stations, again with better agreement at Coastal LA. At Coastal MS. At Coastal MS, it fails to reproduce the low values observed during summer. This bias likely arises from the use of monthly climatological riverine biogeochemical inputs, which cannot resolve sub-monthly variability. Incorporating higher-frequency biogeochemical riverine inputs would likely improve model performance.

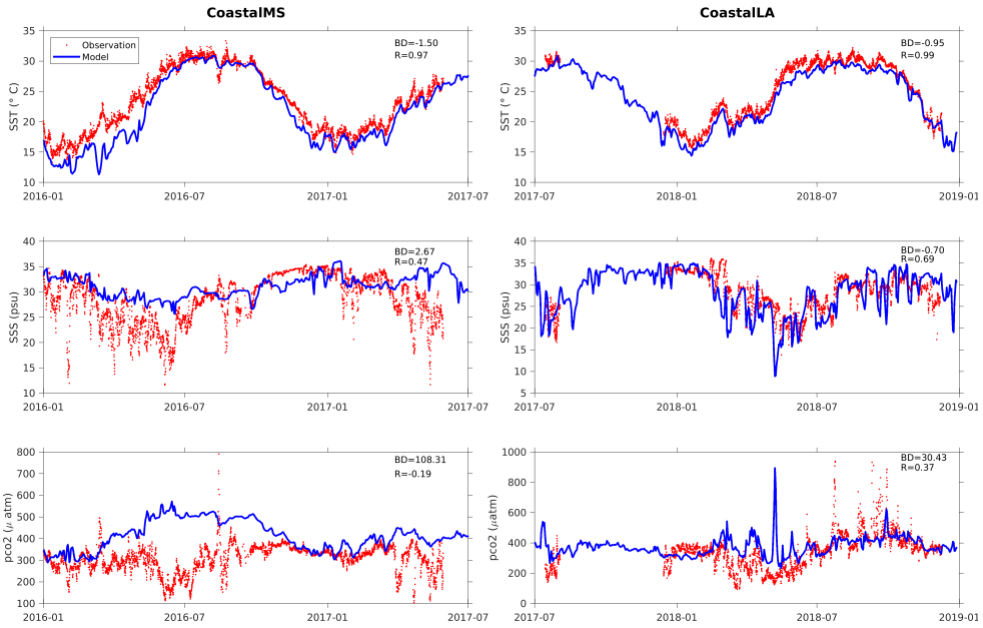

Fig. A2. Time series comparing SST, SSS, and seawater pCO_2 between observations at the Coastal LA and Coastal MS sites and corresponding model outputs.

Satellite-Derived Product Comparisons

Compared with satellite observations, the model reproduces the main spatial and seasonal patterns of chlorophyll in the Northern Gulf (Fig. A3). Observations show high concentrations (>2 mg/m³) in coastal waters, peaking near the Mississippi Delta (>10 mg/m³), and decreasing offshore with depth. The model captures this coastal-to-offshore gradient but produces a broader band of high chlorophyll that extends farther offshore than observed. Model performance in the Florida region is less consistent. Chlorophyll is underestimated along the northern Florida coast and overestimated along the southern Florida coast. Because chlorophyll patterns in this region are strongly influenced by local river inputs, the model biases

are likely attributable to the limited availability and quality of river discharge and riverine biogeochemical tracer data used to represent this region. For the seasonal differences, both observations and the model show high open-sea chlorophyll in winter, though the model tends to overestimate its magnitude.

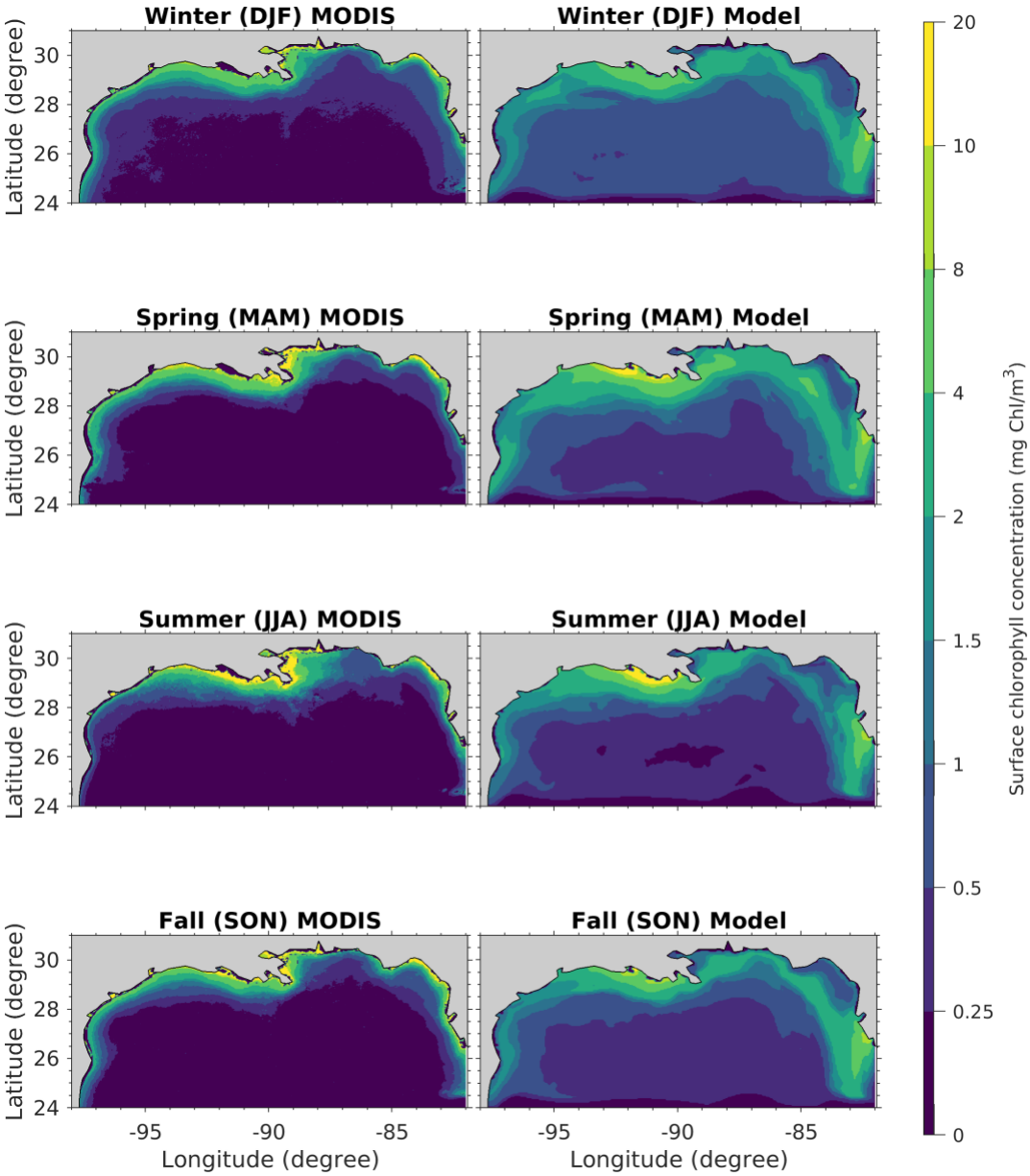

Fig. A3. Modeled surface chlorophyll concentration compared with satellite-derived data, shown as the 2016–2018 seasonal mean average.

Figure A4 compares model-simulated domain-averaged NPP in the open sea (h > 150 m) with satellite-derived estimates from various products. Estimates were limited to the open sea because satellite algorithms perform reliably in clear waters but poorly in turbid coastal regions (Gómez-Letona et al., 2017; Xu et al., 2022). Observed NPP ranges from ~200 to 900 mg C m^{-2} day^{-1}, with higher values in winter and lower in summer. The model reproduces both the magnitude and seasonal cycle, though simulated variability is slightly larger, especially in summer 2016 and winter 2018.

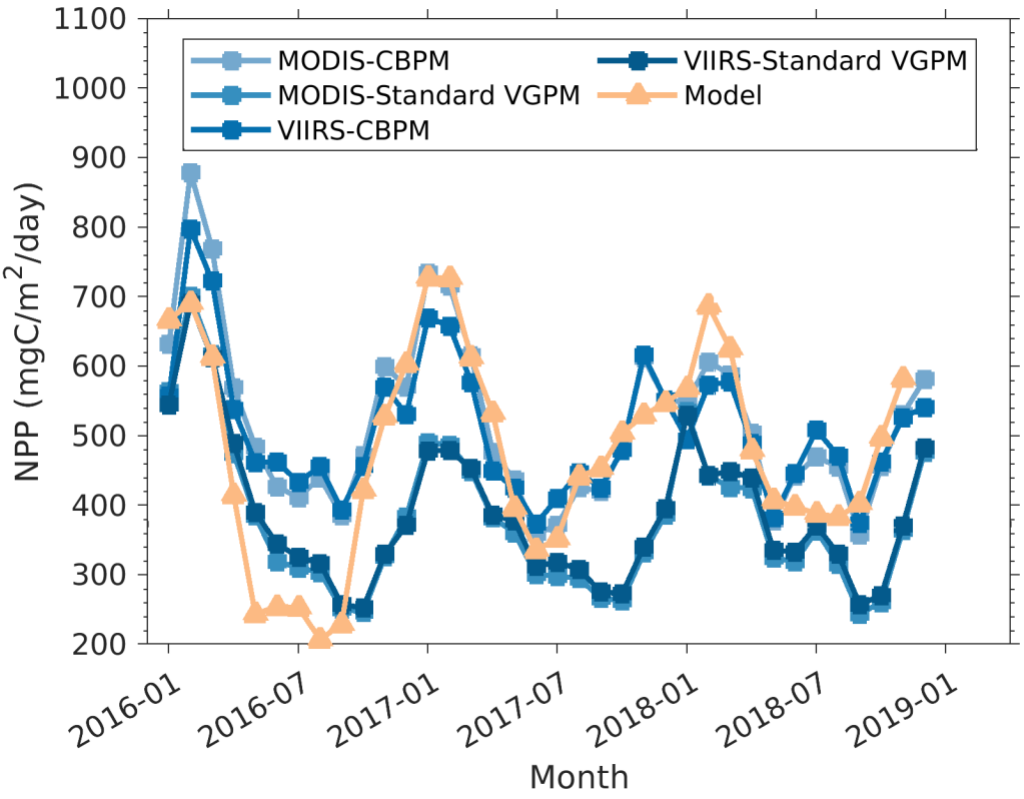

Fig. A4. Comparison between modeled NPP and satellite-derived NPP for the open-sea domain (h > 150 m) of the Northern Gulf.

Cruise-Based Observational Comparisons

Cruise-based observational comparisons to the model were conducted in two ways. First, several cruise trajectories followed roughly linear tracks from the coastal region to the open sea, with multiple measurements taken along each track. These discrete measurements along a single linear trajectory were used to validate model-simulated transects. Because the measurements along a given trajectory were collected over several days, we used the monthly average of the corresponding model output for comparison. Overall, DIC, TA, and their ratio show good agreement (Fig. A5). The model captures the offshore increase of DIC (e.g., Fig. A5a2) as well as the increase of DIC with depth, although it tends to simulate slightly lower DIC values relative to the observations. TA exhibits weaker vertical gradients, and while the model reproduces the magnitude reasonably well, it produces extreme low values in some shallow coastal regions (e.g., Fig. A5a6). For the DIC/TA ratio, observed values are slightly lower than the model, a discrepancy attributable to the model's overestimation of DIC.

Second, all TA and DIC cruise measurements (2,827 data points) were paired with model output at the same locations, depths, and times. These paired datasets were then compared using a whisker plot (Fig. A5b). Result shows that model exhibits a systematic positive bias, with the model overestimating DIC by ~ 40 µmol/kg, and TA by ~20 µmol/kg relative to the median values (red line in Fig. A5b). The DIC/TA ratio is also slightly overestimated, although model values remain within the wide observational range.

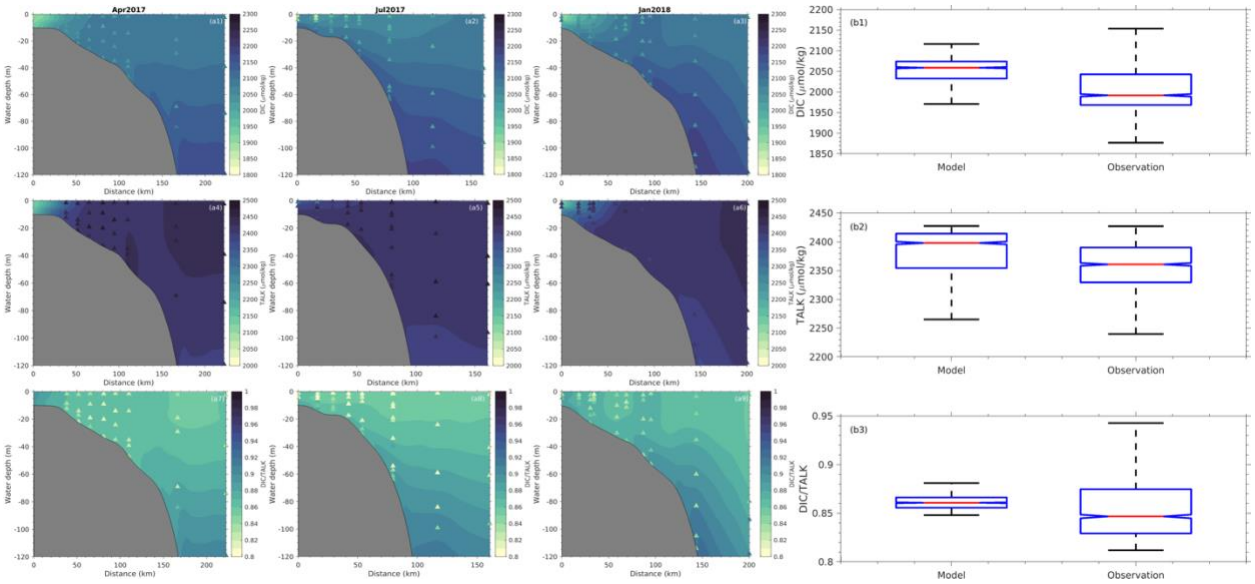

Fig. A5. (a) Example comparison of DIC, TA, and the DIC/TA ratio from cruise measurements (scattered dots) with corresponding model outputs along the cruise transect. (b) Whisker plots comparing all cruise measurements with corresponded model outputs.

SeaFlux Product Evaluation (month ave or value)

Figure A6 shows the three-year averaged spatial distribution of pCO_2 from the SeaFlux product (ensemble mean of six products) and the model output. Both show the same seasonal cycle, with lowest values in winter when the Northern Gulf absorbs atmospheric CO_2 and highest in summer when it outgasses. Compared to SeaFlux, the model simulates slightly lower winter pCO_2 and higher summer values. Spatially, SeaFlux shows lower pCO_2 in coastal regions and higher values offshore, with the lowest near the Mississippi Delta under strong freshwater influence. The model reproduces this gradient but also simulates high pCO_2 near the estuary, a discrepancy expected given the 1° × 1° resolution cannot resolve fine-scale outgassing where river water with high DIC/TA ratios (~1) mixes with ocean water of lower ratios (~0.8). he model also overestimates pCO_2 along the Florida coast, likely due to its poor representation of chlorophyll in that region.

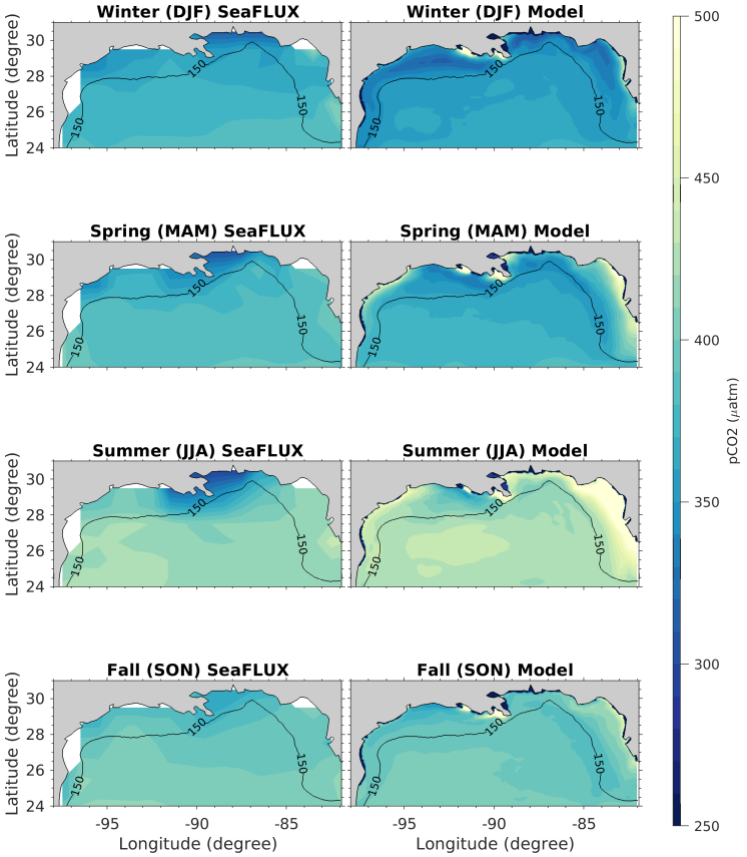

Fig. A6. Comparison of the three-year (2016–2018) seasonal averages of pCO_2 between the SeaFlux ensemble mean and the model output.

Acknowledgment

This work was supported by the United States Department of Energy (DOE) Energy EarthShot Program. AB was partially supported by the European Union's Horizon Europe research and innovation program under grant agreements no. 101056939 (RESCUE). We thank Laure Resplandy and Mathieu Poupon of Princeton University for providing the biogeochemical open boundary conditions and initial fields from the MOM6-COBALT-NWA12 v1.0 simulations, and Andrew Ross of NOAA GFDL for conducting the MOM6-COBALT-NWA12 v1.0 simulations.

Contributions

X.Z., A.B., T.I., C.T.R., conceived the study. X.Z. conducted all model simulations and performed the analyses. X.Z., A.B., T.I., C.T.R. contributed to writing, reviewing, and interpreting the manuscript. All authors have read and approved the final manuscript for submission.

Competing interests

C.T.R. was a co-founder of Lithos Carbon but has no financial ties to the company, and is currently a scientific advisor to CREW Carbon. The authors declare no additional competing interests.

Code and data availability

The CROCO-PISCES model is available at https://www.croco-ocean.org/ . River forcing data can be obtained from https://geo.gcoos.org/river_discharge/ and https://catalog.data.gov/dataset/rc4uscoast-a-river-chemistry-dataset-for-regional-ocean-model-application-in-the-u-s-east-gulf-1. Atmospheric forcing and physical open boundary conditions are available from https://www.hycom.org/dataserver/navgem and https://www.hycom.org/data/goml0pt04. The biogeochemical initial fields and open boundary conditions were extracted from the MOM6-COBALT-NWA12 simulation and can be obtained by contacting the Geophysical Fluid Dynamics Laboratory (GFDL). The model outputs generated specifically for this study are available upon request.

Reference

Archer, D., Kheshgi, H., & Maier-Reimer, E. (1997). Multiple timescales for neutralization of fossil fuel CO2. *Geophysical Research Letters*, *24*(4), 405-408.

Auclair, F., Benshila, R., Debreu, L., Ducousso, N., Dumas, F., Marchesiello, P., Lemarié, F. Some recent developments around the CROCO initiative for complex regional to coastal modeling. In Comod 2018-workshop on coastal ocean modelling (pp. 1-47) (2018, February).

Aumont, O., Éthé, C., Tagliabue, A., Bopp, L., & Gehlen, M. (2015). PISCES-v2: an ocean biogeochemical model for carbon and ecosystem studies. *Geoscientific Model Development Discussions*, *8*(2), 1375-1509.

Babakhani, P., Phenrat, T., Baalousha, M., Soratana, K., Peacock, C. L., Twining, B. S., & Hochella Jr, M. F. (2022). Potential use of engineered nanoparticles in ocean fertilization for large-scale atmospheric carbon dioxide removal. *Nature Nanotechnology*, *17*(12), 1342-1351.

Beerling, D. J., et al. (2020). "Potential for large-scale CO_2 removal via enhanced rock weathering on croplands." Nature, 583, 242–248.

Beerling, D. J., Kantzas, E. P., Lomas, M. R., Taylor, L. L., Zhang, S., Kanzaki, Y., ... & Val Martin, M. (2025a). Transforming US agriculture for carbon removal with enhanced weathering. Nature, 1-10.

Beerling, D. J., Reinhard, C. T., James, R. H., Khan, A., Pidgeon, N., & Planavsky, N. J. (2025b). Challenges and opportunities in scaling enhanced weathering for carbon dioxide removal. Nature Reviews Earth & Environment, 1-15.

Broecker, W. S., & Peng, T. H. (1987). The role of CaCO3 compensation in the glacial to interglacial atmospheric CO2 change. *Global Biogeochemical Cycles*, *1*(1), 15-29.

Burt, D. J., Fröb, F., & Ilyina, T. (2021). The sensitivity of the marine carbonate system to regional ocean alkalinity enhancement. *Frontiers in Climate*, *3*, 624075.

Cao, L., & Caldeira, K. (2010). Atmospheric carbon dioxide removal: long-term consequences and commitment. *Environmental Research Letters*, *5*(2), 024011.

Cummings, J. A.,, Smedstad, O. M. Variational data assimilation for the global ocean. In Data assimilation for atmospheric oceanic, and hydrologic applications (Vol. II) (pp. 303-343). Berlin, Heidelberg: Springer Berlin Heidelberg (2013).

Coles, V. J., Brooks, M. T., Hopkins, J., Stukel, M. R., Yager, P. L., & Hood, R. R. (2013). The pathways and properties of the Amazon River Plume in the tropical North Atlantic Ocean. *Journal of Geophysical Research: Oceans*, *118*(12), 6894-6913.

Davila, X., Gebbie, G., Brakstad, A., Lauvset, S. K., McDonagh, E. L., Schwinger, J., & Olsen, A. (2022). How is the ocean anthropogenic carbon reservoir filled?. *Global Biogeochemical Cycles*, *36*(5), e2021GB007055.

Deng, H., Sonnenthal, E., Arora, B., Breunig, H., Brodie, E., Kleber, M., ... & Nico, P. (2023). The

environmental controls on efficiency of enhanced rock weathering in soils. *Scientific Reports*, *13*(1), 9765.
Duarte, C. M., Losada, I. J., Hendriks, I. E., Mazarrasa, I., & Marbà, N. (2013). The role of coastal plant communities for climate change mitigation and adaptation. *Nature climate change*, *3*(11), 961-968.
Eisaman, M., Geilert, S., Renforth, P., Bastianini, L., Campbell, J., Dale, A., ... & Rønning, J. (2023). Assessing technical aspects of ocean alkalinity enhancement approaches. *State of the Planet Discussions*, *2023*, 1-52.
Fennel, K., Long, M. C., Algar, C., Carter, B., Keller, D., Laurent, A., ... & Whitt, D. B. (2023). Modeling considerations for research on Ocean Alkalinity Enhancement (OAE). *State of the Planet Discussions*, *2023*, 1-47.
Gómez-Letona, M., Ramos, A. G., Coca, J., & Arístegui, J. (2017). Trends in primary production in the canary current upwelling system—A regional perspective comparing remote sensing models. *Frontiers in Marine Science*, *4*, 370.
Gomez, F. A., Lee, S. K., Stock, C. A., Ross, A. C., Resplandy, L., Siedlecki, S. A., ... & Salisbury, J. E. (2022). RC4USCoast: A river chemistry dataset for regional ocean model applications in the US East, Gulf of Mexico, and West Coasts. *Earth System Science Data Discussions*, *2022*, 1-19.
Griscom, B. W., Adams, J., Ellis, P. W., Houghton, R. A., Lomax, G., Miteva, D. A., ... & Fargione, J. (2017). Natural climate solutions. *Proceedings of the National Academy of Sciences*, *114*(44), 11645-11650.
Goodwin, P., & Ridgwell, A. (2010). Ocean-atmosphere partitioning of anthropogenic carbon dioxide on multimillennial timescales. *Global Biogeochemical Cycles*, *24*(2).
Hartmann, J., Suitner, N., Lim, C., Schneider, J., Marín-Samper, L., Arístegui, J., ... & Riebesell, U. (2022). Stability of alkalinity in ocean alkalinity enhancement (OAE) approaches–consequences for durability of CO 2 storage. Biogeosciences Discussions, 2022, 1-29.
Harrington, K. J., Hilton, R. G., & Henderson, G. M. (2023). Implications of the riverine response to enhanced weathering for CO2 removal in the UK. *Applied Geochemistry*, *152*, 105643.
He, J., & Tyka, M. D. (2023). Limits and CO2 equilibration of near-coast alkalinity enhancement. *Biogeosciences*, *20*(1), 27-43.
House, K. Z., House, C. H., Schrag, D. P., & Aziz, M. J. (2007). Electrochemical acceleration of chemical weathering as an energetically feasible approach to mitigating anthropogenic climate change. *Environmental Science & Technology*, *41*(24), 8464-8470.
Intergovernmental Panel on Climate Change (IPCC). (2022). *Global Warming of 1.5°C: IPCC Special Report on Impacts of Global Warming of 1.5°C above Pre-industrial Levels in Context of Strengthening Response to Climate Change, Sustainable Development, and Efforts to Eradicate Poverty*. Cambridge: Cambridge University Press.
Ito, T., & Reinhard, C. T. (2025). A new framework for the attribution of air-sea CO2 exchange. *Global Biogeochemical Cycles*, *39*(2), e2024GB008346.
Jones, D. C., Ito, T., Takano, Y., & Hsu, W. C. (2014). Spatial and seasonal variability of the air-sea equilibration timescale of carbon dioxide. *Global Biogeochemical Cycles*, *28*(11), 1163-1178.
Kaushal, S. S., Likens, G. E., Utz, R. M., Pace, M. L., Grese, M., & Yepsen, M. (2013). Increased river alkalinization in the Eastern US. *Environmental science & technology*, *47*(18), 10302-10311.
Kanzaki, Y., Planavsky, N. J., & Reinhard, C. T. (2023). New estimates of the storage permanence and ocean co-benefits of enhanced rock weathering. *PNAS nexus*, *2*(4), pgad059.
Kanzaki, Y., Planavsky, N. J., Zhang, S., Jordan, J., Suhrhoff, T. J., & Reinhard, C. T. (2025). Soil cation

storage is a key control on the carbon removal dynamics of enhanced weathering. *Environmental Research Letters*, *20*(7), 074055.
Kheshgi, H. S. (1995). Sequestering atmospheric carbon dioxide by increasing ocean alkalinity. *Energy*, *20*(9), 915-922.
Kim, J., Chapman, P., Rowe, G., DiMarco, S. F., & Thornton, D. C. (2020). Implications of different nitrogen input sources for potential production and carbon flux estimates in the coastal Gulf of Mexico (GOM) and Korean Peninsula coastal waters. *Ocean Science*, *16*(1), 45-63.
Lannelongue, L., Grealey, J., & Inouye, M. (2021). Green algorithms: quantifying the carbon footprint of computation. *Advanced science*, *8*(12), 2100707.
Li, Z., Planavsky, N. J., & Reinhard, C. T. (2024). Geospatial assessment of the cost and energy demand of feedstock grinding for enhanced rock weathering in the coterminous United States. *Frontiers in Climate*, *6*, 1380651.
Li, M., Chen, Y., Doyle, R., Testa, J. M., Gagnon, A., Bott, C., & Cai, W. J. (2025). Wastewater alkalinity enhancement for carbon emission reduction and marine CO2 removal. *Environmental Research Letters*, *20*(4), 044041.
Liu, G., Bracco, A.,, Sitar, A. Submesoscale mixing across the mixed layer in the Gulf of Mexico. Frontiers in Marine Science 8, 615066 (2021).
Liu, G., Bracco, A.,, Sun, D. Offshore freshwater pathways in the northern Gulf of Mexico: Impacts of modeling choices. Frontiers in Marine Science 9, 841900 (2022).
Liu, F., Daewel, U., Kossack, J., Demir, K. T., Thomas, H., & Schrum, C. (2025). Evaluating ocean alkalinity enhancement as a carbon dioxide removal strategy in the North Sea. *EGUsphere*, *2025*, 1-34.
Lopera, L., Bracco, A., & Herrera, S. (2025). Physical connectivity between mesophotic areas in the northern Gulf of Mexico. *Journal of Geophysical Research: Oceans*, *130*(2), e2024JC021753.
Luo, H., Bracco, A., Cardona, Y., & McWilliams, J. C. (2016). Submesoscale circulation in the northern Gulf of Mexico: Surface processes and the impact of the freshwater river input. *Ocean Modelling*, *101*, 68-82.
Mu, L., Palter, J. B., & Wang, H. (2023). Considerations for hypothetical carbon dioxide removal via alkalinity addition in the Amazon River watershed. *Biogeosciences*, *20*(10), 1963-1977.
National Academies of Sciences, Medicine, Division on Earth, Ocean Studies Board, Board on Chemical Sciences, Board on Earth Sciences, ... & Reliable Sequestration. (2019). Negative emissions technologies and reliable sequestration: A research agenda.
National Academies of Sciences, Engineering, and Medicine. *A research strategy for ocean-based carbon dioxide removal and sequestration*. 2021.
Moras, C. A., Bach, L. T., Cyronak, T., Joannes-Boyau, R., & Schulz, K. G. (2022). Ocean alkalinity enhancement–avoiding runaway CaCO 3 precipitation during quick and hydrated lime dissolution. Biogeosciences, 19(15), 3537-3557.
Ou, Y., Xue, Z. G., & Hu, X. (2025). A numerical assessment of ocean alkalinity enhancement efficiency on a river-dominated continental shelf—a case study in the northern Gulf of Mexico. *Environmental Research Letters*, *20*(2), 024031.
Paulo, C., Power, I. M., Stubbs, A. R., Wang, B., Zeyen, N., & Wilson, S. (2021). Evaluating feedstocks for carbon dioxide removal by enhanced rock weathering and CO2 mineralization. *Applied Geochemistry*, *129*, 104955.
Raymond, P., Planavsky, N., & Reinhard, C. T. (2025). Using carbonates for carbon removal. *Nature Water*, 1-4.

Regnier, P., Resplandy, L., Najjar, R. G., & Ciais, P. (2022). The land-to-ocean loops of the global carbon cycle. *Nature*, *603*(7901), 401-410.

Renforth, P., & Kruger, T. (2013). Coupling mineral carbonation and ocean liming. *Energy & fuels*, *27*(8), 4199-4207.

Renforth, P., & Henderson, G. (2017). Assessing ocean alkalinity for carbon sequestration. *Reviews of Geophysics*, *55*(3), 636-674.

Ross, A. C., Stock, C. A., Adcroft, A., Curchitser, E., Hallberg, R., Harrison, M. J., ... & Simkins, J. (2023). A high-resolution physical-biogeochemical model for marine resource applications in the northwest Atlantic (MOM6-COBALT-NWA12 v1. 0). *Geoscientific Model Development Discussions*, *2023*, 1-65.

Song, S., Ding, Y., Li, W., Meng, Y., Zhou, J., Gou, R., ... & Lin, G. (2023). Mangrove reforestation provides greater blue carbon benefit than afforestation for mitigating global climate change. *Nature Communications*, *14*(1), 756.

Sun, D., Bracco, A.,, Liu, G. The role of freshwater forcing on surface predictability in the Gulf of Mexico. Journal of Geophysical Research: Oceans 127(5), e2021JC018098 (2022).

Suhrhoff, T. J., Reershemius, T., Wang, J., Jordan, J. S., Reinhard, C. T., & Planavsky, N. J. (2024). A tool for assessing the sensitivity of soil-based approaches for quantifying enhanced weathering: a US case study. Frontiers in Climate, 6, 1346117.

Suselj, K., Carroll, D., Whitt, D., Samuels, B., Menemenlis, D., Zhang, H., ... & Savage, A. (2025). Quantifying marine carbon dioxide removal via alkalinity enhancement across circulation regimes using ECCO-Darwin and 1D models. *Journal of Advances in Modeling Earth Systems*, *17*(7), e2024MS004847.

UNFCCC. (2015). The Paris Agreement (FCCC/CP/2015/L.9/Rev.1).

Wanninkhof, R. (2014). Relationship between wind speed and gas exchange over the ocean revisited. *Limnology and Oceanography: Methods*, *12*(6), 351-362.

Wang, H., Pilcher, D. J., Kearney, K. A., Cross, J. N., Shugart, O. M., Eisaman, M. D., & Carter, B. R. (2023). Simulated impact of ocean alkalinity enhancement on atmospheric CO2 removal in the Bering Sea. *Earth's Future*, *11*(1), e2022EF002816.

Ward, N. D., Bianchi, T. S., Medeiros, P. M., Seidel, M., Richey, J. E., Keil, R. G., & Sawakuchi, H. O. (2017). Where carbon goes when water flows: carbon cycling across the aquatic continuum. *Frontiers in Marine Science*, *4*, 7.

Xu, M., Hu, C., Najjar, R. G., Herrmann, M., Briceno, H., Barnes, B. B., ... & English, D. (2022). Estimating estuarine primary production using satellite data and machine learning. *International Journal of Applied Earth Observation and Geoinformation*, *110*, 102821.

Zhang, S., Reinhard, C. T., Liu, S., Kanzaki, Y., & Planavsky, N. J. (2025). A framework for modeling carbon loss from rivers following terrestrial enhanced weathering. *Environmental Research Letters*, *20*(2), 024014.

Zheng, L. W., Hu, Y., Su, B., Chen, Q. Y., & Liu, J. (2025). The potential of wastewater treatment on carbon storage through ocean alkalinity enhancement. *Science Advances*, *11*(18), eads0313.

Zhou, X., Lopera, L., Roa-Varón, A.,, Bracco, A. Modeling the larval dispersal and connectivity of Red Snapper (Lutjanus campechanus) in the Northern Gulf of Mexico. Progress in Oceanography 224, 103265 (2024).

Zhou, M., Tyka, M. D., Ho, D. T., Yankovsky, E., Bachman, S., Nicholas, T., ... & Long, M. C. (2025). Mapping the global variation in the efficiency of ocean alkalinity enhancement for carbon dioxide removal. *Nature Climate Change*, *15*(1), 59-65.

Supplemental Information

High-resolution numerical assessment of large-scale riverine alkalinity modification scenarios along the southern coast of the United States

Xing Zhou[1, *], Annalisa Bracco[1, 2], Takamitsu Ito[1], Christopher T. Reinhard[1]
[1]School of Earth and Atmospheric Sciences, Georgia Institute of Technology, USA
[2]CMCC Foundation, Euro-Mediterranean Center on Climate Change, Italy.

*Corresponding Author: xzhou473@gatech.edu

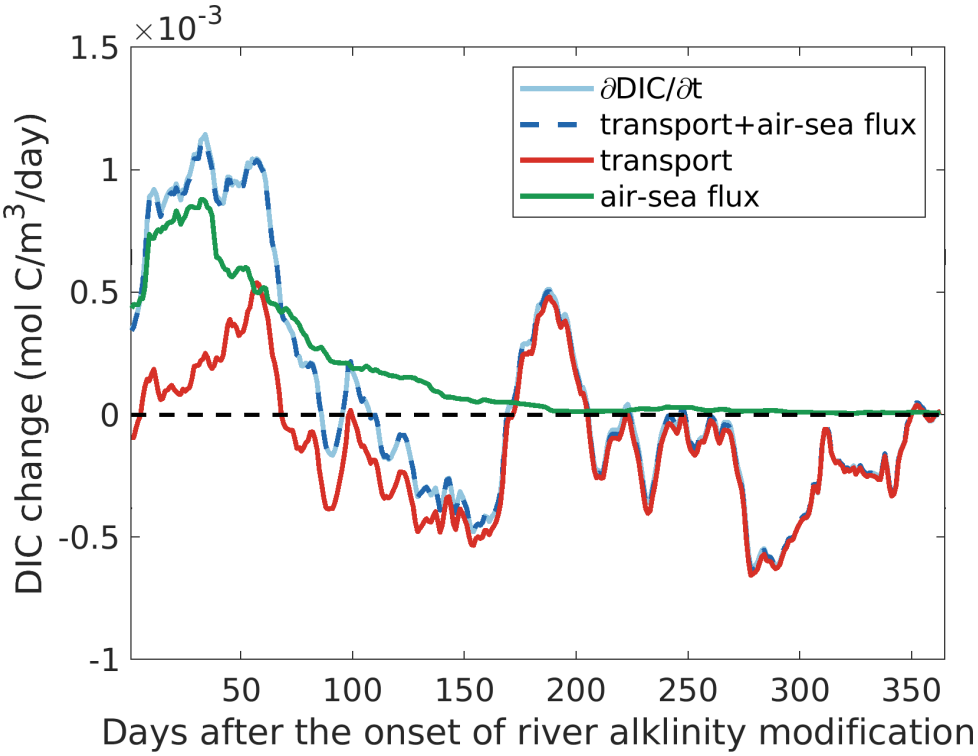

Fig. S1. Diagnostic DIC budget difference (integrated over the entire Gulf) between the Jan100% alkalinity enhancement scenario and the control run. The combined effects of transport (advection and mixing) and air–sea flux differences account for nearly all DIC changes that occurred in 2017. The air–sea flux term shows a clear signal of CO_2 uptake, whereas the transport term primarily reflects noise originating from the open boundary.

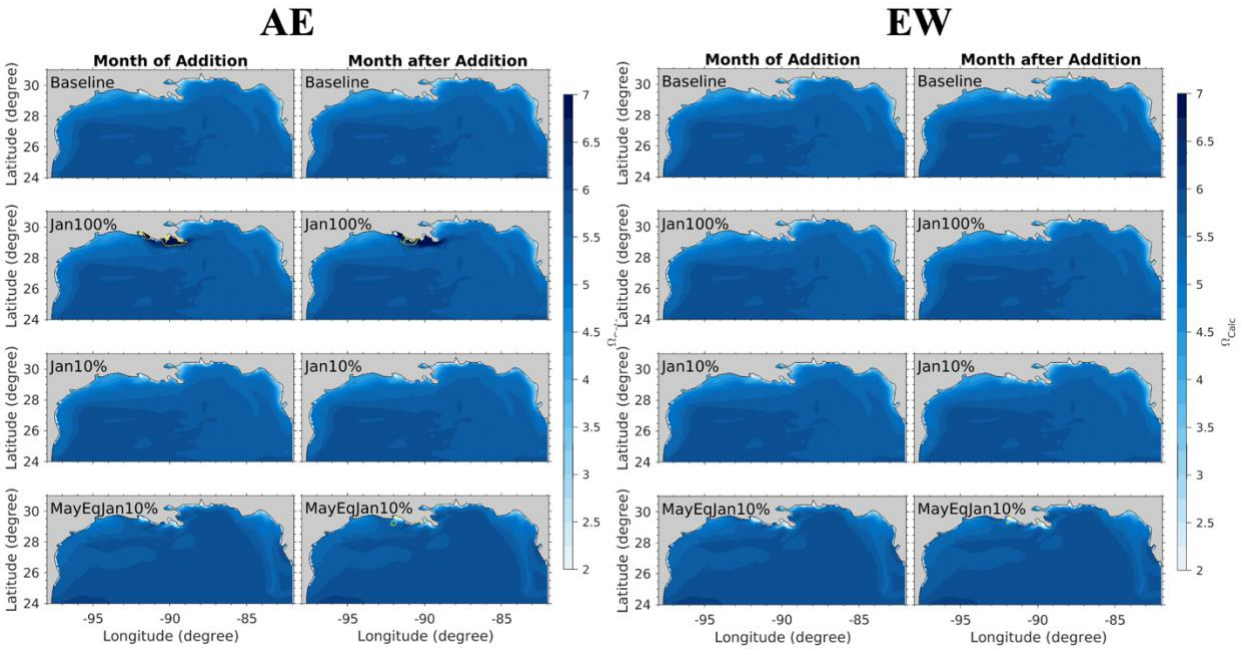

Fig. S2. Spatial distribution of Ω_{Cal} values for the one-month AE and EW pulse scenarios. Results are shown as monthly averages for the month of addition (left panel) and for the following month after the addition ceased (right panel). The yellow line represents the isoline where Ω_{Cal} >7.